Wang et al. Terrestrial, Atmospheric and Oceanic Sciences (2026) 37:15
https://doi.org/10.1007/s44195-026-00132-1

Terrestrial, Atmospheric and Oceanic Sciences

RESEARCH Open Access

Evaluation of multi-member ensemble quantitative precipitation forecasts in the Taiwan Area Heavy-rainfall Prediction Experiment (TAHPEX) for dry-run Mei-yu events: higher predictability over mountains than plains in Taiwan

Chung-Chieh Wang[1*], Po-Yu Huang[1], Jing-Shan Hong[2], Fang-Ching Chien[1], Ming-Jen Yang[3], Ling-Feng Hsiao[2], Chien-Her Chen[2], Shin-Hau Chen[1], Chih-Sheng Chang[1], Pay-Liam Lin[4], Rosimar Rios-Berrios[5], Ching-Yuang Huang[4], Bill Skamarock[5], Guo-Yuan Lien[2], Pi-Yu Chuang[1], Cheng-Chin Liu[2], Shin-Yi Huang[1], Bo-Xun Lin[2], Yi-Wen Wang[1], Chin-Tzu Fong[2] and Guo-Chen Leu[2]

Abstract

In this study, the skill of 24—h quantitative precipitation forecasts (QPFs) for nine verification periods in three Mei-yu events during dry-runs by the cloud-resolving multi-model ensemble (with grid sizes of roughly 1 – 3 km) in the Taiwan Area Heavy-rainfall Prediction Experiment (TAHPEX) is evaluated. Categorical statics of threat score (TS) and bias score (BS) at thresholds of 50 – 350 mm (per 24 h) are employed, for QPFs out to five days at most. Overall, the members show improvements in QPF skills compared to previous forecast verification studies, with TS reaching at least 0.22 at 0 – 24 h, 0.19 at 24 – 48 h, and 0.15 at 48 – 96 h at thresholds of 130 mm and below. The TSs are only slightly lower at 200 mm, but in general ≤ 0.1 at 350 mm. The lead time with some skill is also extended to beyond three days. Most members, however, under-predict heavy rainfall with BS < 1, more serious toward higher thresholds, at ranges close to 48 – 72 h and beyond, and over the plain areas (≤ 300 m in elevation) compared to the mountains (> 300 m). A key result of the present work is that the skill of QPFs and thus the predictability is significantly higher over the mountains in Taiwan than the plains, as a large component of mountain rainfall is phase-locked and stationary. Thus, the mountain regions consistently exhibit higher TSs, BSs closer to 1 (with less under-prediction), and higher probabilities of heavy rainfall derived from the ensemble runs across all members, lead times, and thresholds examined. Among the ensemble products, the exceedance probability from the most-rainy member often has higher TSs than all other products, including probability matching, because it has the

*Correspondence:
Chung-Chieh Wang
cwang@ntnu.edu.tw

Full list of author information is available at the end of the article

least under-forecast and can over-forecast. It is more useful over the mountains. Finally, the finer 1—km members, executed only once per day, show good potential for further improvement to QPFs in heavy-rainfall scenarios.

Keywords Quantitative precipitation forecast, Heavy rainfall, Mei-yu, TAHPEX project, Categorical statistics, Taiwan

1 Introduction

Situated at the center of the East Asian monsoon system and the periphery of western North Pacific (e.g., Wang 2006; Zhou et al. 2011), Taiwan is prone to heavy rainfall due to its high and steep mesoscale topography (Fig. 1a) and often abundant moisture supply (e.g., Chien and Kuo 2011; Wang et al. 2013, 2021a, 2022a), brought by tropical cyclones (July–October, e.g., Wu and Kuo 1999; Chien et al. 2008; Su et al. 2012; Chang et al. 2013) or Mei-yu fronts and southwesterly flow in early summer (May–June, Kuo and Chen 1990; Jou et al. 2011). These events cause flash floods and landslides in the mountain region and inundation in populous cities over coastal plains (e.g., Hsu et al. 2010; Wang et al. 2013; Wang AH et al. 2021). Therefore, accurate heavy-rainfall quantitative precipitation forecasts (QPFs) by numerical models are in great demand in Taiwan (and other regions under similar conditions), and yet their improvement is a challenging task (e.g., Mullen and Buizza 2001; Fritsch and Carbone 2004; Clark et al. 2009; Cuo et al. 2011).

During the past decade or so, it has been demonstrated that heavy-rainfall QPFs in Taiwan can be improved considerably by using cloud-resolving models (e.g., Wang 2015; Wang et al. 2021b) at high resolution with at least a convective-permitting capability (e.g., Liu et al. 1999; Braun 2002; Done et al. 2004; Clark et al. 2009). This also includes the Mei-yu season. For example, Wang et al. (2022b) showed that the Cloud Resolving Storm Simulator (CReSS, Tsuboki and Sakakibara 2002, 2007), with a grid size (Δx) of 2.5 km, achieved threat scores (TSs, see details in Sect. 2.3) of 0.23, 0.16, and 0.15 at rainfall thresholds of 100, 200, and 350 mm on day 1 (0 – 24 h), 0.19, 0.16, and 0.07 on day 2 (24 – 48 h), and 0.15, 0.06, and 0.03 on day 3 (48 – 72 h), respectively, for roughly the largest 20% of Mei-yu events during 2012 – 2014. Named group A, these events were those with ≥ 10% of rain gauges reaching 50 mm (per 24 h) and thus excluded smaller events. Although lower than those for typhoons (e.g., Wang et al. 2021b, 2023a, 2025a), such skills for Mei-yu QPFs are no doubt higher than those obtained by 5—km models in operation at the time (also Wang et al. 2025b). Thus, increasing model resolution is very helpful for heavy-rainfall QPFs in Taiwan.

Since the atmosphere is a nonlinear system and all forecasts contain errors to limit the predictability (e.g., Lorenz 1963; Epstein 1969; Hohenegger and Schär 2007; Shen et al. 2021), the multi-member ensemble approach is often adopted at operational centers to assess forecast uncertainty and better cover all possible scenarios (e.g., Toth and Kalnay 1993; Eckel and Mass 2005), including the Central Weather Administration (CWA) of Taiwan using the Weather Research and Forecasting (WRF) model (Skamarock et al. 2005; Hsiao et al. 2013; Hong et al. 2015; Powers et al. 2017). While desired, such an approach obviously requires much larger computational resources than a single model would, particularly when cloud-resolving capability is not to be sacrificed. Besides the CWA, such an effort was put forward before by the Taiwan Typhoon and Flood Research Institute (TTFRI) during 2011 – 2018, but their ensemble members, including WRF and also Mesoscale Model version 5 (MM5, Grell et al. 1994; Dudhia 2005), were again all at 5—km grid size, except the sole member of the 2.5—km CReSS (Wang 2015; Wang et al. 2021b, 2022b).

Since 2019, in collaboration with the Taiwan Area Heavy rain Observation and Prediction Experiment (TAHOPE, Yang et al. 2026), the integrated project of Taiwan Area Heavy-rainfall Prediction EXperiment (TAHPEX) is setup in Taiwan to support each other. On one hand, the TAHOPE conducted the field campaign and modeling studies related to data assimilation (DA). On the other hand, while TAHPEX has its own modeling component in science (excluding DA), it also has an application component to build a cloud-resolving, multi-model ensemble system and provide real-time predictions for the field operation of TAHOPE. The overall goal of TAHPEX is to improve the understanding of physical processes and predictability of Mei-yu and typhoon, and the QPF skills for extreme/heavy rainfall in Taiwan. Due to the outbreak of the global pandemic in early 2020, the TAHOPE field campaign was delayed for two years and eventually successfully conducted from 25 May to 10 August in 2022 (Yang et al. 2026). From 2019 to 2021, dry runs during the Mei-yu season were carried out, when TAHPEX also provided real-time forecasts. The TAHPEX project combines the resources of public, academic, and research sectors, and the cloud-resolving multi-model ensemble at Δx of around 3 km (and up to 1 km for some members) is a logical next step to improve heavy-rainfall QPFs in line with the past efforts up to around 2020 as reviewed above (e.g., Wang et al. 2022b). In this study, the QPF results for three dry-run heavy-rainfall events are reported.

Given the above background of TAHPEX, the main goals of the present study are threefold and listed below:

1. To assess the QPF capability by cloud-resolving members in TAHPEX for Mei-yu heavy rainfall and

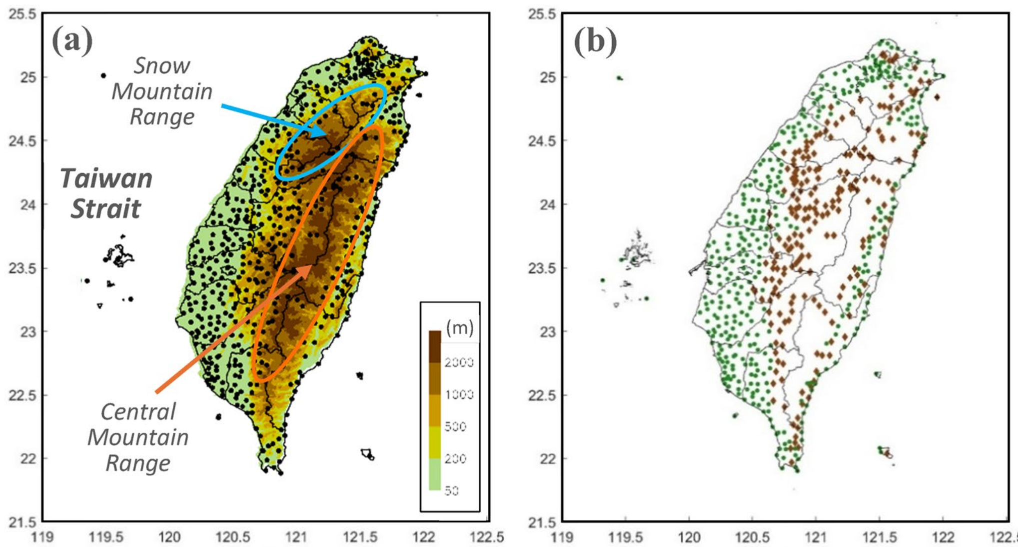

Fig. 1 (**a**) The topography of Taiwan (m, color) and the distribution of rain gauges (dots) in 2021, with Taiwan Strait and the two major mountain ranges, Central Mountain Range (CMR) and Snow Mountain Range, marked, and (**b**) gauge sites over the plains (green dots, 390 sites) and those over the mountains (brown diamonds, 221 sites)

evaluate whether progresses are made compared to earlier modeling/QPF efforts

2. To explore how different ensemble products can be beneficial for Mei-yu QPFs
3. To demonstrate the different predictability of rainfall over mountains compared to that over the plains in Taiwan

From long-term experience and many case studies in the past, heavy rainfall in the mountain regions of Taiwan (under southwesterly flow) is known to be more frequent, and more importantly, phase-locked to the topography (e.g., Fang and Kuo 2011; Jou et al. 2011; Yu and Cheng 2013; Wang et al. 2022a, 2025b), whereas the rainfall over the low-lying plains near the coast is produced by transient systems under the influence of the front and/or local circulation (e.g., Davis and Lee 2012; Wang et al. 2021a, 2023b). Thus, the predictability of rainfall in Taiwan should be significantly higher with better skill over the mountains than the plains, but we believe that this difference has not been properly demonstrated in the literature. Therefore, this aspect is chosen as our third goal.

For the remaining part of this paper, Sect. 2 describes the TAHPEX experiment during dry-run periods, the data, and methodology for QPF verification. For each of the three selected heavy-rainfall events, an overview and verification results are presented and discussed in Sects. 3, 4, and 5, respectively. In Sect. 6, further discussion linked to our first goal is offered. Finally, a summary and the conclusions are given in Sect. 7.

2 Data and methodology

2.1 The TAHPEX project and dry-run Mei-yu events

During 2019 – 2021, TAHOPE and TAHPEX carried out dry-run trial experiments in the first half of June, which is the most-rainy period of the season in Mei-yu climatology (e.g., Chi 2006; Yeh and Chen 1998; Wang et al. 2017; Wang AH et al. 2021). In addition, the extreme event in early June 2017 (e.g., Wang et al. 2021a, 2023b; Tu et al. 2022) was included in the project as a special case. Eventually, nine target periods (i.e., forecast verification periods) from three events that met the 200 mm (per 24 h) heavy-rainfall criterion of the CWA were chosen for study, as the statistics of the season at heavy-rainfall thresholds would be more or less dominated by these major events, as shown in Wang et al. (2022b). These events are 1 – 4 June 2017 (event 1), 10 – 14 June 2019 (event 2), and 29 May – 1 June 2021 (event 3), respectively.

The major specifications of TAHPEX members that provided data in this study is given in Table 1. Members M01-M05 have a Δx of 2.5 or 3 km, close to the suggested grid size by Gentry and Lackmann (2010) and similar to the recommendation of a small-size, high-resolution (4 km) ensemble by Fang and Kuo (2013). From a nested domain of a global model, the grid size of M10 is around 4.8 km and slightly coarser (Chen et al. 2024; Lin et al. 2026). At $\Delta x = 1$ km, M11 and M13 have the finest grid, but their forecasts were made only once per day at 1200 UTC. As operational models at the CWA, M04 and M05 (Hsiao et al. 2015, 2020) had routine runs every 6 h, while the remaining members were run twice per day at 0000 and 1200 UTC, with M01 providing an additional run at 1800 UTC in 2021. For each event, data from certain

Table 1 Major specifications of TAHPEX members to provide data in this study, including member number, model (with institution), horizontal grid size Δ*x*, vertical levels, frequency, forecast range, initial and boundary condition (IC/BC), DA, cloud microphysics scheme (with number of moments), cumulus parameterization scheme, and planetary boundary layer (PBL) scheme. The E1, E2, and E3 in parentheses denote events 1 – 3 in 2017, 2019, and 2021, respectively, and + 18 Z in the frequency of M01 means an additional run at 1800 UTC. Abbreviations for those not yet defined in text are given at the bottom

Member	Model	Δx (km)	Vertical levels	Frequency (runs/day)	Range (h)	IC/BC	DA	Cloud microphysics	Cumulus parameterization	PBL
M01	NTNU CReSS	2.5	40	2 (E1, E2) 3 (E3, + 18 Z)	120	NCEP GFS	No	Cold rain (1.5)	No	Deardorff
M02	NTNU WRF	3.0	45	2	96 (E1) 120 (E2, E3)	NCEP GFS	No	Goddard	Tiedtke	YSU
M03	NTU WRF	3.0	41	2	96	NCEP GFS	No	WDM6 (2)	Kain-Fritsch	YSU
M04	CWA WRF-D	3.0	52	4	84 (E1) 120 (E2, E3)	NCEP GFS	Yes	Goddard	Kain-Fritsch	YSU
M05	CWA TWRF	3.0	52	4	84 (E1) 120 (E2, E3)	NCEP GFS	Yes	Goddard	Kain-Fritsch	YSU
M10 (E2, E3)	CWA TGFS*	~ 4.8	63	2	120	NCEP GFS	No	GFDL	No	TKE-EDMF
M11 (E1, E2)	NTNU CReSS1	1.0	45	1 (12 Z)	96	NCEP GFS	No	Cold rain (1.5)	No	Deardorff
M13 (E2, E3)	CWA SUM	1.0	42	1 (12 Z)	102 (E2), 120 (E3)	NCEP GFS	No	WSM3 (1)	No	MRF

* M10 was from the nested domain of an earlier version of the CWA TGFS before it had become operational since 2023. Unlike the operational configuration, neither the DA nor cumulus parameterization was used during the experiment periods included in this study.

For model: WRF-D (deterministic WRF), TWRF (Typhoon WRF), TGFS (Taiwan Global Forecast System), SUM (Spectral Unified Model); For IC/BC: NCEP (National Centers for Environmental Prediction), GFS (Global Forecast System); For cloud microphysics: WDM6 (WRF double-moment 6 class), GFDL (Geophysical Fluid Dynamics Laboratory), WSM3 (WRF single-moment 3 class); For PBL: YSU (Yonsei University), TKE-EDMF (turbulent kinetic energy-based moist eddy-diffusion mass-flux), MRF (Medium-Range Forecast) model.

Table 2 Available number of runs from TAHPEX members at each initial time window (12 h apart) for each of the 24—h verification periods in the three events, respectively. The runs by M04 and M05 at 0600 UTC (1800 UTC) are grouped into the ensemble runs at 1200 UTC (0000 UTC) 6 h later, and the same is for M01 runs at 1800 UTC in event 3. The verification periods (24 h each) start at the last time with a number, which is highlighted in bold face

Event 1 (2017)					Event 2 (2019)				Event 3 (2021)		
Initial time	P1	P2	P3	P4	Initial time	P1	P2	P3	Initial time	P1	P2
5/31 00 Z	5	5	5	5	6/6 12 Z	3			5/25 12 Z	4	
12 Z	8	8	8	8	6/7 00 Z	3			5/26 00 Z	5	
6/1 00 Z	7	7	7	7	12 Z	3	3		12 Z	5	5
12 Z	**8**	8	8	8	6/8 00 Z	3	3		5/27 00 Z	5	5
6/2 00 Z		**7**	7	7	12 Z	3	3		12 Z	5	5
12 Z			**8**	8	6/9 00 Z	6	6	6	5/28 00 Z	5	5
6/3 00 Z				**7**	12 Z	10	10	10	12 Z	5	5
					6/10 00 Z	8	8	8	5/29 00 Z	5	5
					12 Z	**8**	8	8	12 Z	**4**	4
					6/11 00 Z		8	8	5/30 00 Z		5
					12 Z		**10**	10	12 Z		**9**
					6/12 00 Z			6			
					12 Z			9			
					6/13 00 Z			**8**			

members might not be available. Also note that the forecast ranges lie between 84 and 120 h, so some members might not have outputs for verification toward the longest lead times for some target periods. While many acronyms are given at the bottom of the table, the readers are referred to the papers cited above, Powers et al. (2017), Wang et al. (2023a), and their official websites for further details of the models and their configurations, including the domain size. Nonetheless, the specifications and configurations both vary to large extents among all members, so we tend not to focus on their individual performance, but the performance of the entire ensemble system in later discussion.

With the range and frequency listed in Table 1, Table 2 summarizes the forecast runs available for each of the qualified 24—h target periods in the three events. These periods start at 1200 UTC 1 June, 0000 UTC and 1200 UTC 2 June, and 0000 UTC 3 June 2017 in event 1 (denoted as P1 – P4, respectively), 1200 UTC 10 June, 1200 UTC 11 June, and 0000 UTC 13 June 2019 (P1 – P3) in event 2, and 1200 UTC 29 May and 1200 UTC 30 May (P1 and P2) in event 3, respectively. In event 1, overlapping of target periods occurred using the 200—mm criterion because its rainfall episodes were lengthy enough. As relatively few runs were executed at 0600 and 1800 UTC, those at such times are grouped into the ensemble at 0000 or 1200 UTC 6 h later, applying the time-lagged concept (e.g., Mittermaier 2007; Lu et al. 2007; Yuan et al. 2008; Trilaksono et al. 2012; Wang et al. 2021a, 2023c). Thus, the 0000 and 1200 UTC in our study in fact refer to a time window (6 h in length) instead of fixed times.

2.2 Observational data for analysis and QPF verification

The observational data during the events used in this study include the following. The CWA weather maps at various levels are used for synoptic analysis of weather patterns. Satellite infrared (IR) cloud imageries are used to depict rainfall systems, and rainfall data (at hourly intervals) from a dense network of manned stations and automated rain gauges over Taiwan (Fig. 1b), also provided by the CWA (Hsu 1998), are summed to show 24—h rainfall distributions as well as to verify model QPFs. To demonstrate the difference in predictability, these sites are classified into those over the plains (elevation $\le$ 300 m) and in the mountains (elevation $>$ 300 m, see Fig. 1b). In 2017, 2019, and 2021, the plain sites increased from 340, to 369, then to 390, while the numbers of mountain sites were 179, 209, and 221. Thus, the total site numbers were 519, 578, and 611, respectively.

2.3 Methods for QPF verification

In order to assess the skill level of QPFs by the TAHPEX members compared to past results in Taiwan and fulfill our first research goal, the conventional categorical statistics (e.g., Wilks 2011; Ebert et al. 2003) are adopted as the primary method of verification. Thus, based on event occurrences (rainfall reaching a given threshold) in the observation (*O*) and/or forecast (*F*), the outcomes at all verification points (*N*) can be grouped into four categories in the 2×2 contingency table: hits (*H*, event in both in *O* and *F*), misses (*M*, event in *O* but not *F*), false alarms (*FA*, event in *F* but not *O*), and correct negatives (event in neither *O* nor *F*), respectively. From the table, the two widely-used scores, the TS and bias score (BS), can be computed as (Schaefer 1990, with examples; Jolliffe and Stephenson 2003)

$$\text{TS} = H/(H+M+FA), \text{ and} \tag{1}$$

$$\text{BS} = (H+FA)/(H+M) \tag{2}$$

Thus, the TS (with a value between 0 and 1) is a measure of how well the observed rainfall area is predicted and the higher, the better. The BS measures whether the model over-forecast (BS > 1) or under-forecast (BS < 1) the size of the rain area, with the most ideal value being one. While more details can be found in the references cited above, one often needs to choose suitable thresholds and avoid issues like the double penalty in space and time (e.g., Ebert and McBride 2000; Davis et al. 2006; Wang et al. 2023a). As our focus is on heavy-rainfall QPFs, later verification results are at thresholds chosen from 50, 80, 130, 200, 250, and 350 mm per 24 h. Among them, 80, 200, and 350 mm correspond to the CWA criteria for "heavy rainfall" and increasingly larger events (https://www.cwa.gov.tw/V8/C/K/CommonFaq/rain_all.html). In TAHPEX, all model data were interpolated onto a common grid of 0.025° × 0.025° (roughly 2.5 km × 2.5 km) for real-time transfer, then interpolated again onto the gauge sites to perform the verification in this work, as in many earlier studies. So, the same procedure was applied to all members for data processing.

Several ensemble products are also produced and evaluated, and Table 3 provides an explanation of how each one is computed. These include the ensemble mean, and the rainfall using probability matching (PM) technique (e.g., Ebert 2001; Fang and Kuo 2013) to remedy the issue of smoothing out peak values by the ensemble mean. The exceedance probability (EP) refers to the rainfall amount to exceed certain probability in the ensemble, such as top 10% of members (e.g., Fawcett and Walshaw 2013). Owing to the small size of the TAHPEX ensemble, only the rank is used and EP-1, EP-2, and EP-3 refer to the member with the highest, second highest, and third highest rainfall (Table 3), respectively. Thus, EP-1 would correspond to the top 10% in a 10-member ensemble, but the top 1/3, or 33%, if only three runs were available at a given lead time.

Table 3 The post-processing methods for five different ensemble products in this study, including the ensemble mean, PM, and exceedance probability at rank 1 (EP-1), rank 2 (EP-2), and rank 3 (EP-3), respectively

Mean	Arithmetic average of all members
PM	Rank all rainfall at all grid points by all the members inside the verification domain from high to low, then extract the median value from each batch of ensemble size and assign it to the grid point from high to low (i.e., the value from the *i*th batch to the *i*th grid point), at the order of the ensemble mean
EP-1	Use the highest rainfall value among all members at every grid point
EP-2	As in EP-1, except using the second highest rainfall value
EP-3	As in EP-1, except using the third highest rainfall value

3 Event 1: 1—4 June 2017

3.1 Event overview

The first event took place over 1–4 June 2017. The surface Mei-yu front approached Taiwan slowly from the north on 1 June, with a series of mesoscale convective systems (MCSs) developing along it (Fig. 2a). The front moved to central Taiwan and lingered during 2–3 June (Fig. 2b,c), before moving to the south and weakening on 4 June (figure not shown). At low levels, strong west-southwesterly flow of 20–35 kts persisted near and upstream of Taiwan throughout 1–3 June at 850 hPa (Fig. 2d–f). The flow was even stronger farther aloft, and gradually turned into westerlies of about 30–50 kts at 500 hPa (Fig. 2g–i).

The evolution of the convection and MCSs near the Mei-yu front during event 1 is depicted by the IR cloud imageries every 6 h in Fig. 3. Leading to 1200 UTC 1 June, the series of active MCSs along the front was apparent (Fig. 3a, b), and further intensified as the associated rainband made landfall in northern Taiwan around 1800 UTC (Fig. 3c; e.g., Wang et al. 2021a, 2023b). As the rainband stalled across the northern coast, clear back-building behavior was evident near 0000 UTC 2 June, with new cells triggered in succession at the western end of the band over northern Taiwan Strait (Fig. 3d). This rainband eventually produced a peak amount of 635 mm over 12 h in northern Taiwan. Finally, the front and its convection started to move south just before 0600 UTC 2 June (Fig. 3e), with new MCS development in central Taiwan Strait, producing rainfall in central Taiwan including the coastal plains from 1200 UTC 2 June to 0000 UTC 3 June (Fig. 3f – h). During this period, new cell development upstream (to the west) of existing MCSs was again evident. During 3 June, another large MCS developed over southern Taiwan Strait, and then moved onshore to central and southern Taiwan (Fig. 3i – k). Only on 4 June, convection started to weaken, finally bringing this event to an end (Fig. 3l, later figures not shown). The extreme rainfall event along the northern coast has been studied by Wang et al. (2021a, 2023b) and Tu et al. (2022).

With the active MCSs and convection during 1 – 3 June as reviewed above (Fig. 3), heavy rainfall was received in many regions in Taiwan, both in mountain interiors and

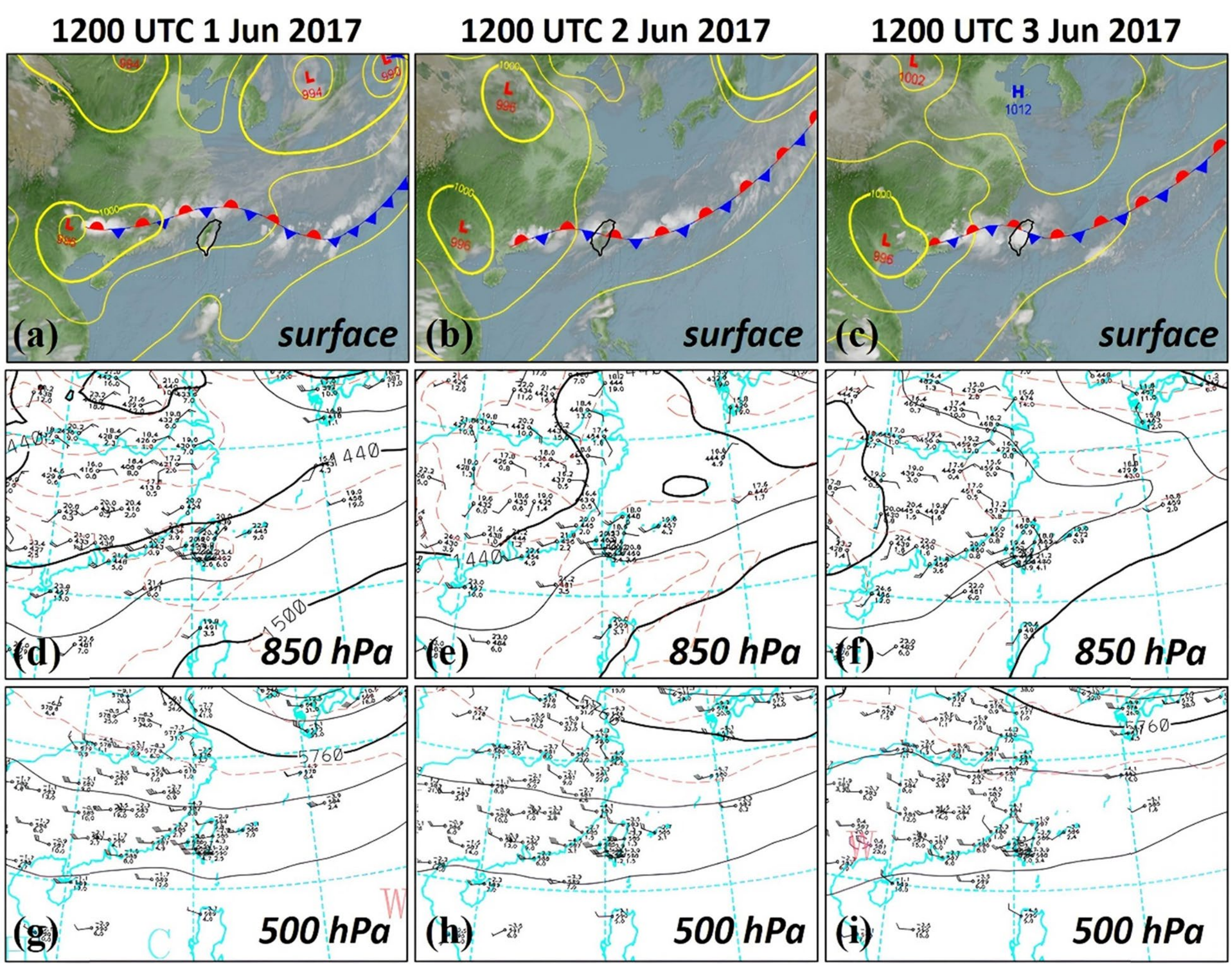

Fig. 2 The color surface weather maps produced by the CWA every 24 h at 1200 UTC of (**a**) 1 June, (**b**) 2 June, and (**c**) 3 June 2017, respectively, with isobars drawn every 4 hPa (yellow, thickened at 1000 hPa). (**d**) – (**f**) As in (**a**) – (**c**) except at 850 hPa, with geopotential height analyzed every 30 gpm (black contours) and isotherms (red dashed) drawn every 3 °C. (**g**) – (**i**) As in (**d**) – (**f**) except at 500 hPa, with height contours every 60 gpm and isotherms every 5 °C. Station plots and wind barbs follow the convention

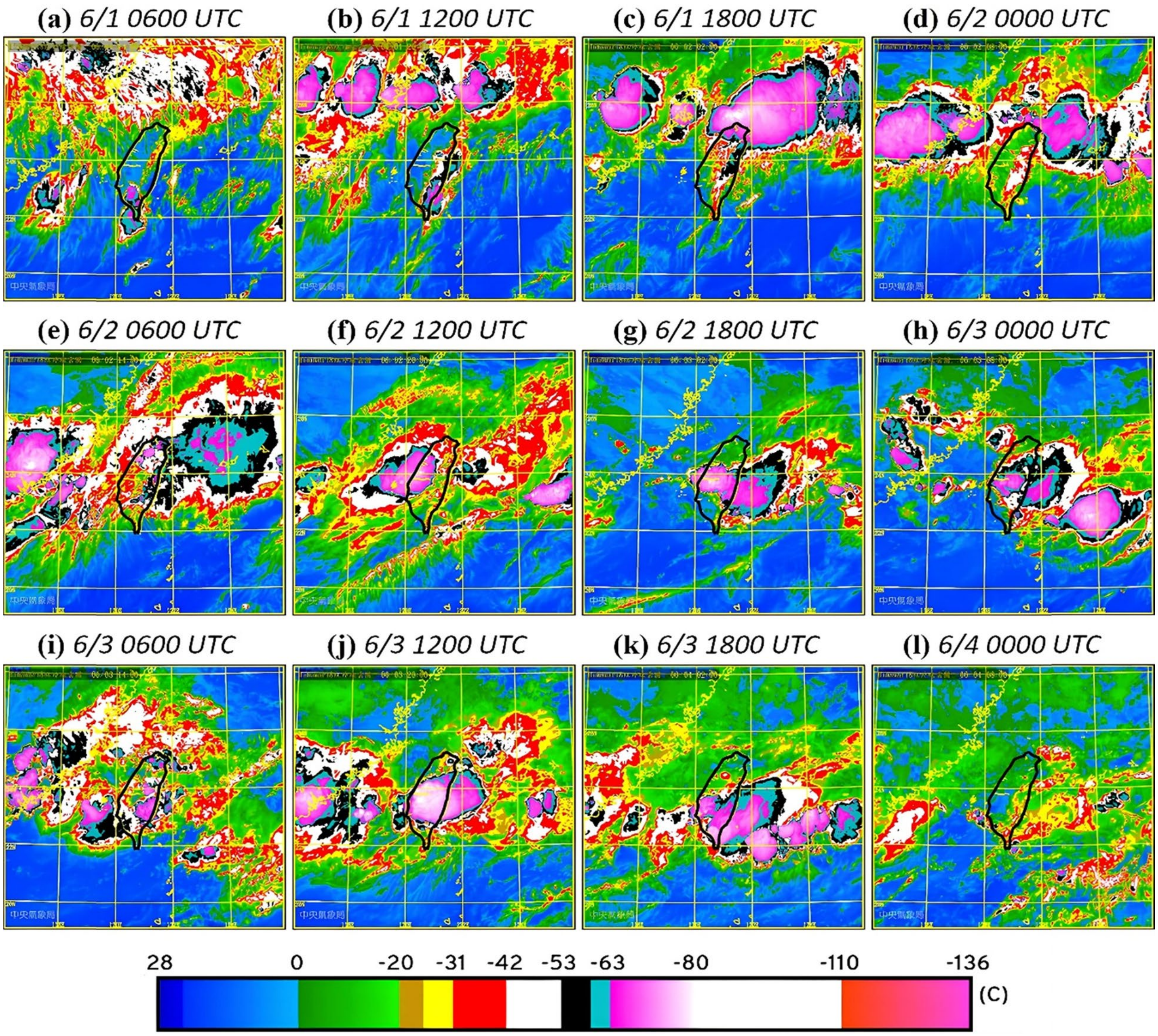

Fig. 3 Geostationary satellite IR cloud imagery (brightness temperature, °C, scale at bottom) surrounding Taiwan every 6 h from (**a**) 0600 UTC 1 June to (**l**) 0000 UTC 4 June 2017 during event 1

over the plains (Fig. 4). From 1200 UTC 1 June to 1200 UTC 2 June, heavy rainfall occurred along the northern coast (peaking at 645 mm), central CMR (~ 400 mm), and southern CMR (519 mm, Fig. 4a). On 2 June (in UTC, Fig. 4b), the rainfall stopped in northern Taiwan (~ 250 mm) after a few hours, while the peak amount in the southern CMR reached 643 mm, over 300 mm in central CMR, and up to 505 mm in central plain near the foothill (near 23.7°N, 120.6°E), caused by the MCSs seen in Fig. 3f – h. From 1200 UTC 2 June to 1200 UTC 3 June (Fig. 4c) and also on 3 June (0000 – 2400 UTC, Fig. 4d), the two centers merged into one in central-southern CMR and the maximum rainfall accumulations were 657 and 609 mm over each of those time periods, respectively. Meanwhile, the rain over central plains and northern Taiwan gradually reduced. These four 24—h periods are the target periods for QPF verification in event 1, which was a special case for re-run in TAHPEX due to its extreme rainfall. With 12 h of overlapping, the sample size is enlarged for event 1 to increase the stability of the verification results.

3.2 Verification of QPFs

Using the method described in Sect. 2.3, the categorical scores of QPFs (starting from 0000 UTC 31 May with no missing runs, Table 2) by each member and ensemble products are computed at different forecast ranges for each verification period. For the overall results, contingency tables at the same threshold and range for different target periods are combined into one table to compute the scores. In Figs. 5 and 6, the overall TS and BS of TAHPEX members for event 1 are shown as a function

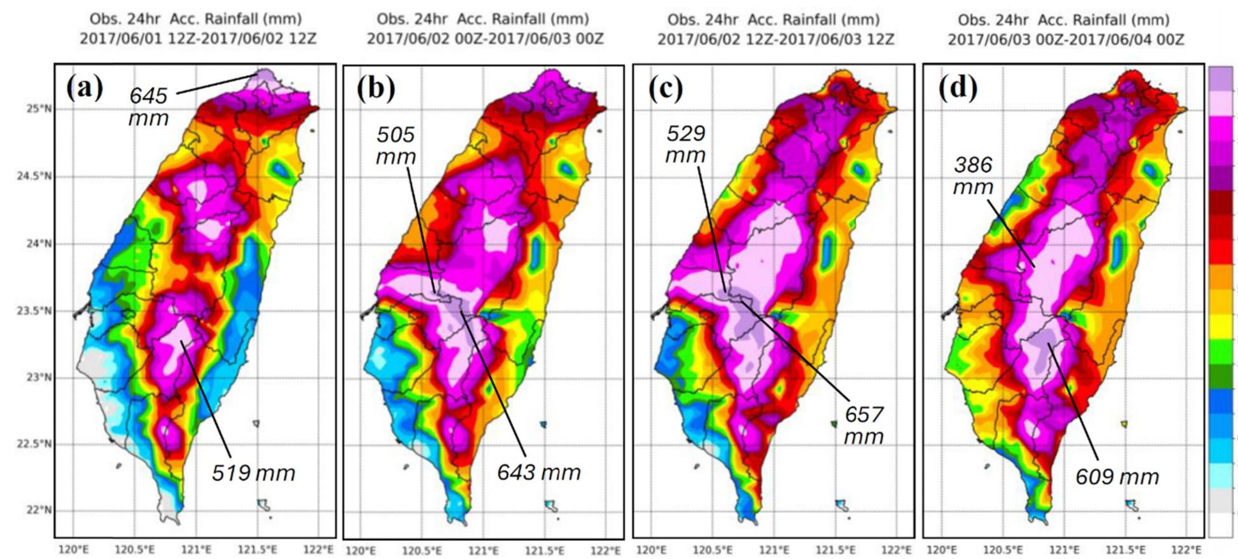

Fig. 4 The observed 24—h rainfall distribution (mm, scale to the right) over Taiwan (**a**) from 1200 UTC 1 June to 1200 UTC 2 June, (**b**) over 0000 – 2400 UTC 2 June, (**c**) from 1200 UTC 2 to 1200 UTC 3 June, and (**d**) over 0000 – 2400 UTC 3 June 2017 during event 1, respectively

of forecast range (i.e., lead time) at a few selected thresholds from 80 to 350 mm. While some members perform better and others less so, we do not focus on their differences since their configurations are considerably different (Table 1). Typically, the TSs increase as the forecast lead time shortens (Fig. 5), but the 12 – 36 h QPFs tend to be the best compared to 0 – 24 h ones, presumably linked to spin-up issues of rainfall systems. For event 1, this is the case even for one member with DA in M05. As the threshold rises, the TSs drop lower, and the overall TS of 12 – 36 h QPFs (from all sites) is around 0.5 at 80 mm, 0.27 at 200 mm, 0.18 at 250 mm, and below 0.05 at 350 mm. When the QPFs for mountain rainfall (middle column) are compared with those over the plains (right column), the former is significantly better than the latter across all thresholds and lead times, and the TS results for the entire Taiwan lie in between the two. With the finest grid ($\Delta x = 1$ km), M11 tends to perform better in TSs from its daily runs, especially at range beyond day 1 and out to day 3.5 (60 – 84 h). Among other members, M03 also performs quite well.

In Fig. 6a, the overall BSs of most members at 80 mm for the entire Taiwan are close to unity within the range of 2 days, with some under-prediction over 0 – 24 h, in agreement with the spin-up. At ranges beyond 48 h, however, under-forecast in rainfall becomes more and more serious. This tendency is also evident toward higher thresholds, as the BSs among all four ranges within 36 – 60 h drop to about 0.7 at 200 mm, and further to only around 0.25 at 350 mm (Fig. 6d,g). Thus, even at resolutions higher than before, the TAHPEX members still struggle to produce enough rainfall for extreme Mei-yu cases in Taiwan like event 1, leading to lowered TSs. In the mountain region (middle column), the characteristics of BSs are similar to those in the whole island, with increasing under-prediction toward higher thresholds and longer lead times. Over the plains (right column), however, individual members may sometimes over-forecast rainfall at certain ranges to offset the under-forecast in the mountains, especially M11 and even at 350 mm. Even so, over-forecasts (over plains) are still rare compared to under-forecasts, and only occur in some members at some lead times. Nevertheless, with a finer grid, M11 is indeed more capable to produce more intense rainfall from migratory MCSs, suggesting potential benefits to further increase model resolution.

The overall TSs obtained from ensemble products at the same thresholds are shown in Fig. 7. The characteristics of the TSs are similar to those in Fig. 5 in many aspects. The ensemble mean and PM have a slight advantage at 80 mm at the two shortest ranges, 0 – 24 and 12 – 36 h (Fig. 7a). At longer ranges and higher thresholds, EP-1 emerges as having the highest TS among all products, while the ensemble mean is often the worst as expected. Again, the TSs over the mountains are consistently higher than those over the plains across all thresholds shown, by large margins as well. While the TSs of EP-1 may not be quite as high as the best member in Fig. 5 (at the same threshold and range), but its certainty offers practical value in real-time operations since the best member is not known in advance.

As for the BSs of ensemble products, the mountain areas often have more ideal values (closer to 1) at 80 and 200 mm within the range of 36 – 60 h compared to the plains and Taiwan as a whole (Fig. 8a – f), because the members do not tend to under-forecast or it is less

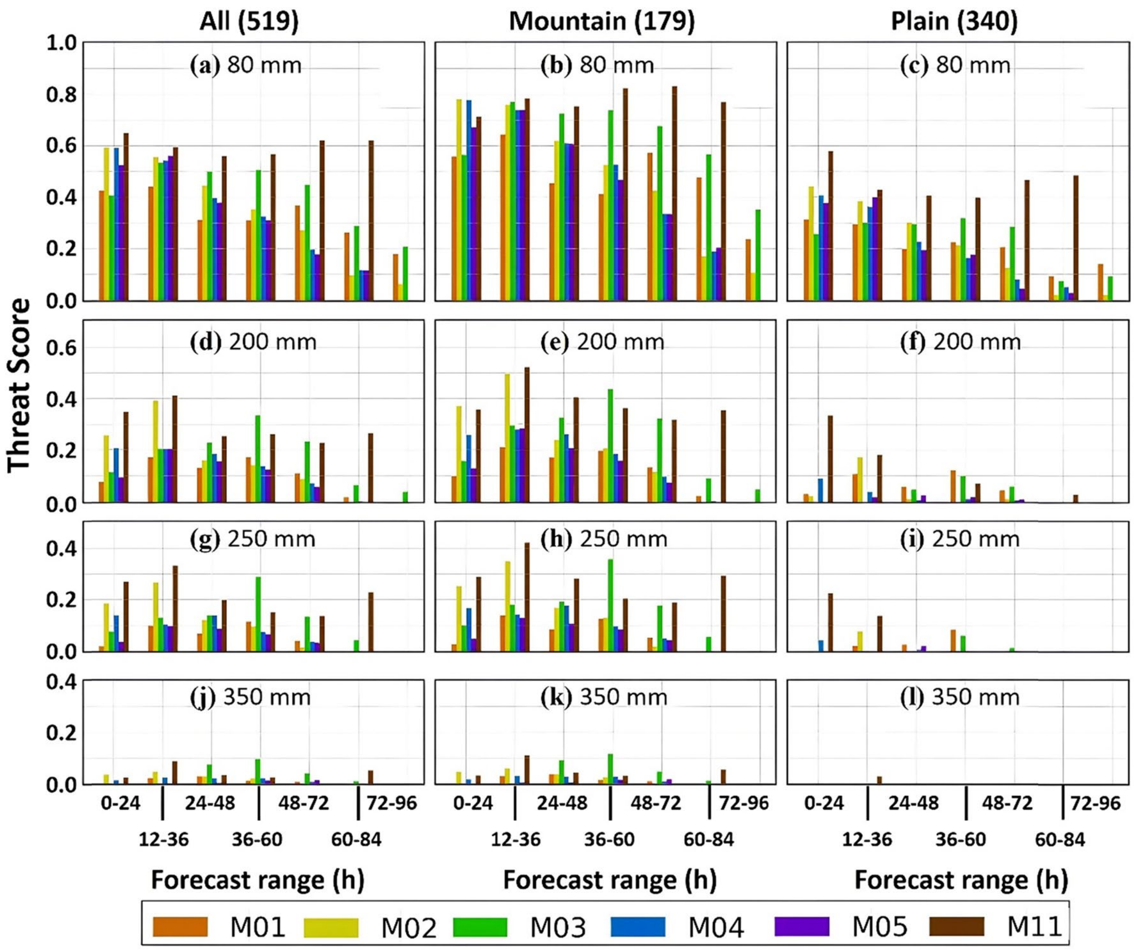

Fig. 5 TS values of 24—h QPFs in event 1 made by the TAHPEX members as a function of forecast range (every 12 h from 0 – 24 to 72 – 96 h), combined for the four target periods, at the threshold of 80 mm, computed at (**a**) all (519) gauge sites in Taiwan, (**b**) mountain sites (179), and (**c**) plain sites (340) only, respectively. Second to fourth rows as in (**a**) – (**c**), except at thresholds of (**d**) – (**f**) 200 mm, (**g**) – (**i**) 250 mm, and (**j**) – (**l**) 350 mm, respectively, as labelled. Legend for the members is shown at the bottom

serious. However, none of the products shows a consistent advantage here, as the BS closest to 1 can be from any one of them. At longer ranges and toward higher thresholds, EP-1 always has the least under-prediction (or slight over-prediction, Fig. 8h, k) in the mountain areas and thus often emerges as having the highest TS. However, over the plains, EP-1 frequently exhibits serious over-prediction (right column), except at longer lead times or above 250 mm. In such cases, the BSs from EP-2, EP-3, or PM may be better. Because of this, EP-1 for the entire island may also over-predict rainfall (left column), except at 350 mm and ranges beyond 48 h, while most other products under-predict. In any case, from Figs. 5, 6, 7 and 8, the TSs for event 1 are seen to be much higher over the mountains where the predictability is higher, than the plain areas with lower predictability associated with mostly transient MCSs.

3.3 Example of ensemble rainfall probability

One other useful tool from ensemble forecasts is the probability of certain events, as shown in Fig. 9 from runs for period 3 at selected initial times at 0000 or 1200 UTC (which includes the previous 0600 or 1800-UTC runs) as an example. While the probabilities of 24—h rainfall reaching different thresholds gradually increase as the lead time shortens, those over the mountains remain higher than over the plains (e.g., northern Taiwan and central coastal plain, cf. Figure 1) rather consistently for areas that actually hit those thresholds in the observation (black contours, Fig. 9). This is again an indication that the rainfall predictability is higher over the mountains. However, at 350 mm, no more than 20 – 40% of members could produce such an amount even in the mountains no matter the lead time, and almost none of them could reach 500 mm, consistent with the under-forecast in this rather extreme event.

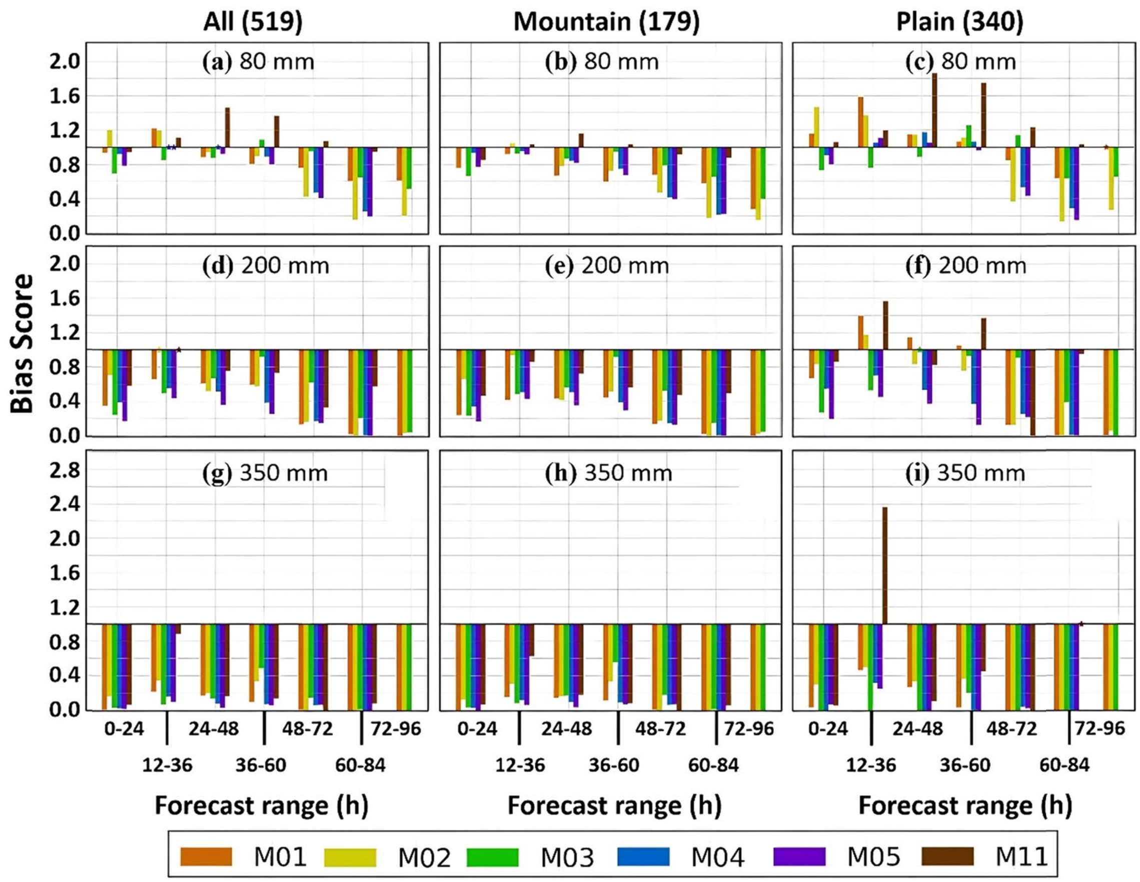

Fig. 6 As in Fig. 5, except showing the BS values in event 1 at (**a**) – (**c**) 80 mm, (**d**) – (**f**) 200 mm, and (**g**) – (**i**) 350 mm, respectively

4 Event 2: 10—14 June 2019

4.1 Event overview

The second event occurred during 10–14 June 2019 as the Mei-yu front lingered near Taiwan. The surface front was nearly stationary just north of Taiwan at 1200 UTC 10 June (Fig. 10a), then moved southward slowly to reach southern Taiwan at 1200 UTC 11 June (not shown) and 0000 UTC 12 June (Fig. 10b). Afterwards, the front retreated and stayed near northern Taiwan until 0000 UTC 13 June, when a frontal low developed (Fig. 10c). Then, the high-pressure system behind the front strengthened and pushed the front to advance southward across Taiwan on 14 June 2019 (not shown). From 850 to 500 hPa, the prevailing winds shifted from west-southwesterly to almost westerly, and were stronger at 1200 UTC 10 June (around 25 – 40 kts, Fig. 10d, g) than 0000 UTC 12 June (about 20 – 25 kts, Fig. 10e, h). At 0000 UTC 13 June, the low-to-mid-level flow strengthened again in association with the developing low (Fig. 10f, i).

On satellite IR cloud imageries, the convection near the Mei-yu front became more active prior to 1800 UTC 10 June (Fig. 11a, b), and a large MCS developed and reached maturity around 0000 UTC 11 June (Fig. 11c) to affect central Taiwan. After this MCS weakened and diminished (Fig. 11d,e), the front moved south and new MCSs broke out over the southern Taiwan Strait around 1800 UTC 11 June (Fig. 11f). As convection continued to develop over Taiwan through 0600 UTC 12 June (Fig. 11g, h), the surface front retreated northward. Then, as the low developed, the front moved through Taiwan for the second time on 13 June, producing another wave of deep convection in Taiwan (Fig. 11i – l).

The accumulated rainfall distributions in Taiwan over three 24—h periods (P1 – P3) are shown in Fig. 12. The first is from 1200 UTC 10 June to 1200 UTC 11 June, with three rainfall centers in northern (~ 120 mm), central (307 mm), and southwestern Taiwan (173 mm), from the MCSs seen in Fig. 11a – d. The rain fell mainly in central CMR (270 mm) as the front retreated during the second period (Fig. 12b), from 1200 UTC 11 June to 1200 UTC 12 June, but the central plain also received some rainfall (162 mm). During P3 on 13 June (in UTC), three centers in northwestern plain (235 mm), central CMR, and southern CMR (224 mm) were observed, as the Mei-yu front swept through Taiwan. For event 2, these are the three target periods for QPF verification.

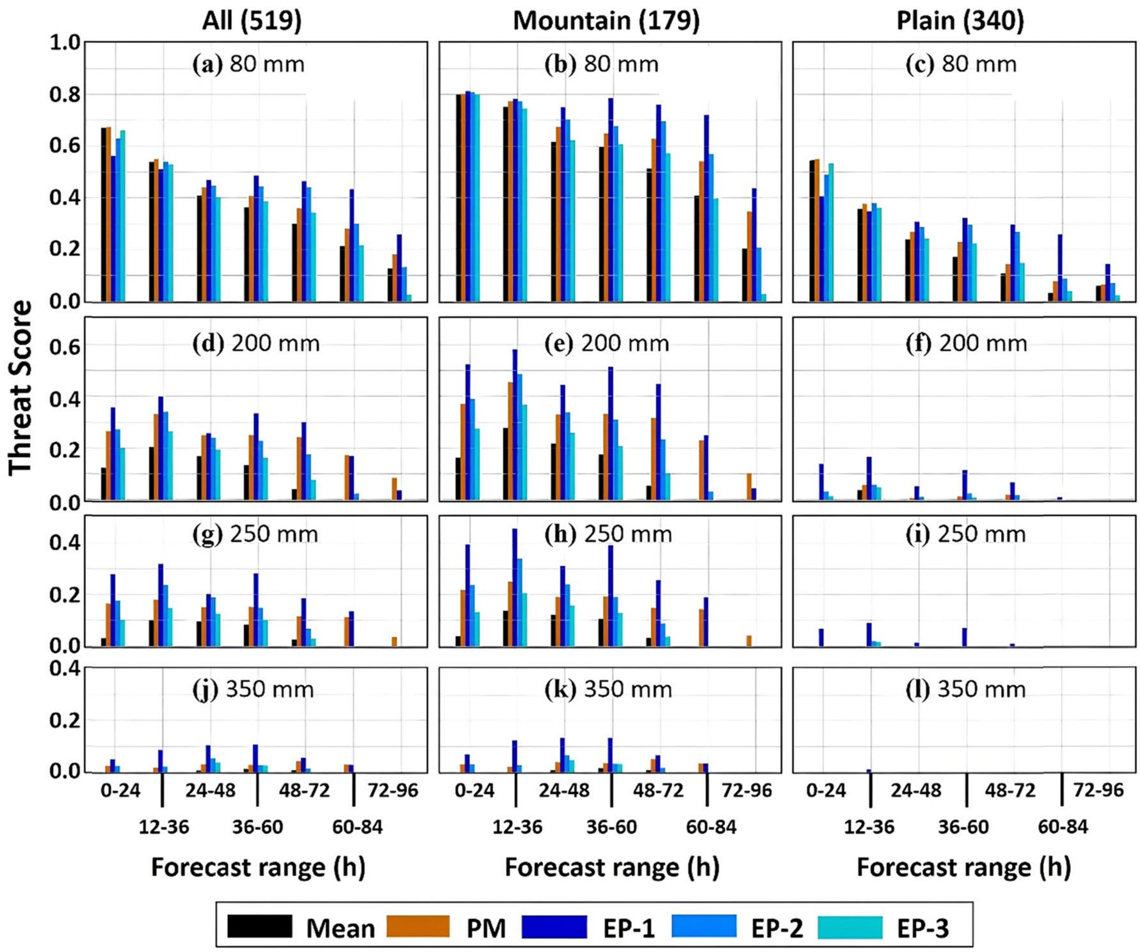

Fig. 7 As in Fig. 5, except showing the TS values of TAHPEX ensemble products in event 1, including ensemble mean, PM, EP-1, EP-2, and EP-3 as a function of forecast range (every 12 h from 0 – 24 to 72 – 96 h) at the threshold of (**a**) – (**c**) 80 mm, (**d**) – (**f**) 200 mm, (**g**) – (**i**) 250 mm, and (**j**) – (**l**) 350 mm, respectively. Legend for the products is at the bottom

4.2 Verification of QPFs

For event 2, data from M01, M02, and M10 became available from the runs at 1200 UTC 6 June and those from M04 and M05 were from 0000 UTC 9 June 2019. The two 1—km members, M11 and M13, were since 1200 UTC 9 June (Table 2). Measuring the accuracy of QPFs, the overall TSs for event 2, with contingency tables integrated over P1 – P3, are depicted in Fig. 13 at four thresholds from 50 to 200 mm. Generally, the scores are higher at 0 – 24 h than 12 – 36 h. Toward the longer range, the 1—km members (M11 and M13) and a few other ones could at times make better QPFs, even at 96 – 120 h. For event 2, however, its TSs at 50 mm are roughly comparable to those at 80 mm in event 1, and most of them at 130 mm are already lower than those at 200 – 250 mm in event 1. At 200 mm, no member exhibits any skill (TS > 0) at ranges beyond day 2 (Fig. 13j – l). Thus, the overall skill is lower in event 2 compared to event 1 mainly because it was a smaller rainfall event (Figs. 4 and 12), in agreement with Wang (2015) and Wang et al. (2022b). Again, the TSs over the mountains (209 sites) are mostly higher than over the plains (369 sites) across all thresholds and ranges in event 2, with only occasional exceptions.

The BSs (which measure under/over forecasting) corresponding to Fig. 13 are presented in Fig. 14, but results at the threshold of 200 mm are omitted. At just 50 mm, the majority of members already show under-prediction in rainfall over the entire Taiwan for event 2 except at the shortest range on day 1 (Fig. 14a). This tendency worsens toward longer ranges and becomes the most serious near 48 – 72 h (mean BS ≈ 0.3), then somewhat less serious farther beyond. Toward higher thresholds (Fig. 14d, g), the under-prediction of most members also becomes worse. At times, some members could produce BS > 1 across the thresholds and achieve higher TSs in Fig. 13 (including M11 and M13), particularly when the over-forecasting is not too serious (say, BS ≤ 2). Nevertheless, many members seriously under-predict while others excessively over-predict rainfall, and this happens more frequently over the plains than the mountains (middle

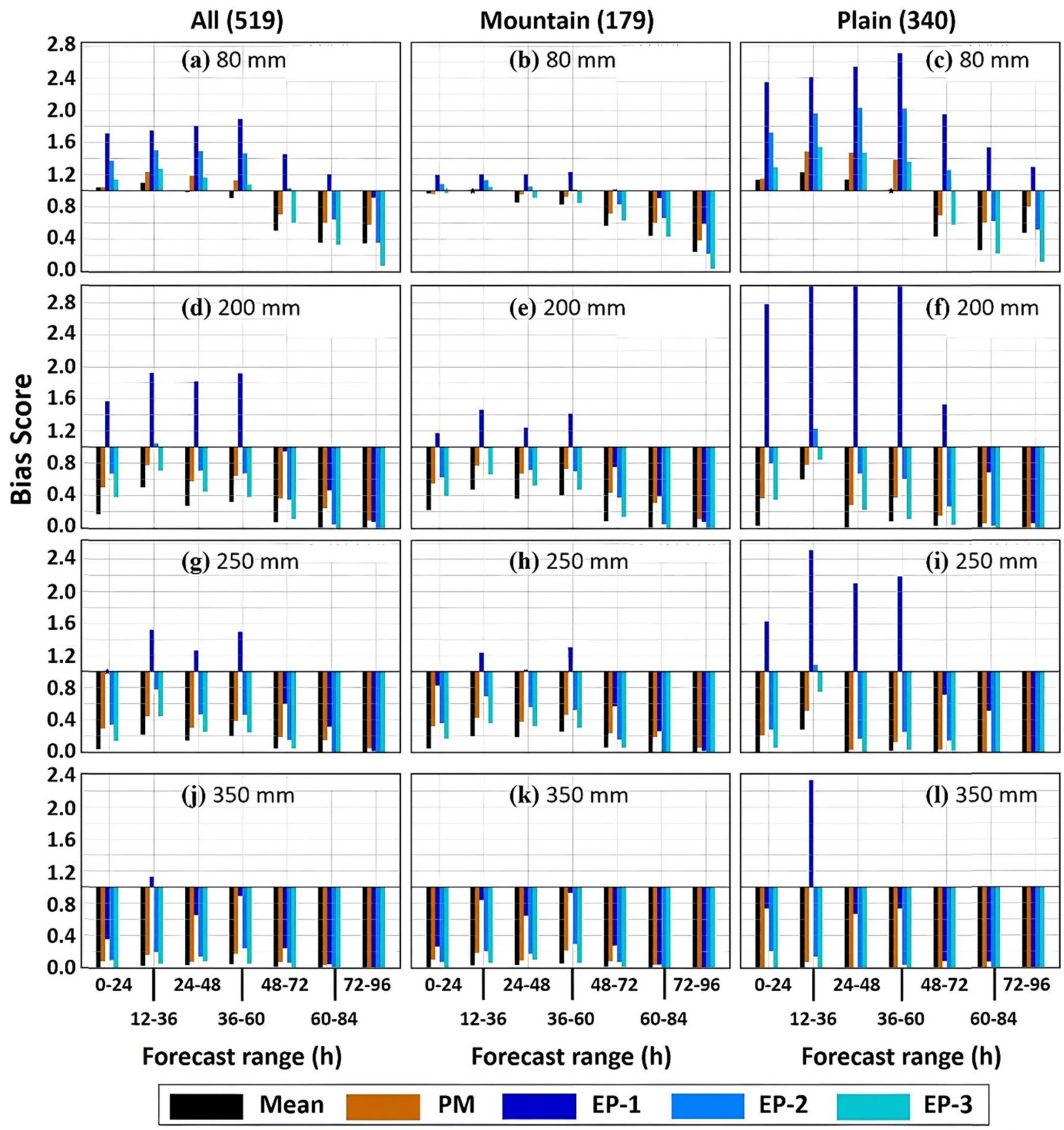

Fig. 8 As in Fig. 7, except showing the BS values in event 1 at (**a**) – (**c**) 80 mm, (**d**) – (**f**) 200 mm, (**g**) – (**i**) 250 mm, and (**j**) – (**l**) 350 mm, respectively

and right columns), again suggesting a lower predictability with more unstable QPF results in the plains. At 200 mm (BS not shown), the above contrasting condition also worsens but all TS = 0 over the plains (see Fig. 13l), thus no hit occurs there even when roughly 1/3 of members over-predict rainfall. In this aspect, the condition is less serious over the mountains.

The TSs of ensemble products for event 2 are shown in Fig. 15, again consistently better over the mountains than the plains. Compared to the TSs by individual members (Fig. 13), they tend to be better across all ranges at 50 and 80 mm for all three regions (Fig. 15a – f). The differences in TSs among these products are often quite limited within 12 – 36 h at 50 and 130 mm and 0 – 24 h at 80 mm, but the EP-1 always has the best TSs beyond these ranges, often even higher than the best member at 50 mm. Toward higher thresholds, this may not be true but EP-1 remains competitive against most members. At 200 mm, slightly more products register TS > 0 than the members, but they do not help over the plains where no member is effective. Another likely advantage of ensemble products is that their performance is more stable across the forecasts. From Fig. 16, it is clear that the better performance in TSs by EP-1 for event 2 (for which most members under-predict rainfall) is mainly because it raises the BS significantly (and increase hits) at ranges beyond about 12 – 36 h. At shorter ranges, the BSs of EP-1 are often excessive and PM, EP at a lower rank, or

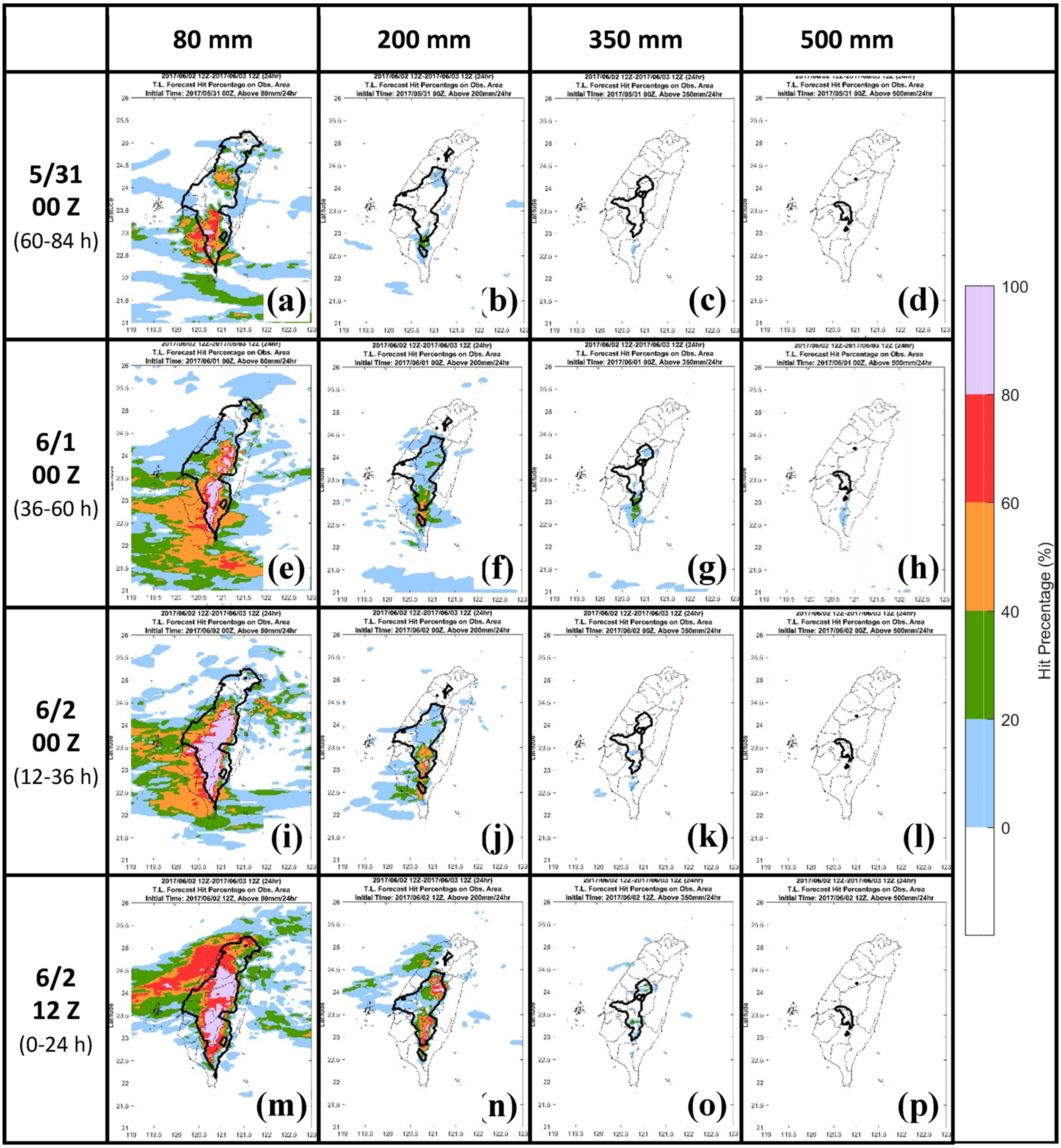

Fig. 9 Ensemble probabilities of 24—h QPFs (%, color, scale to the right) from all members initialized at 0000 UTC 31 May 2017 to reach (**a**) 80, (**b**) 200, (**c**) 350, and (**d**) 500 mm for target period 3 (1200 UTC 2 to 1200 UTC 3 June) in event 1. Remaining rows as in (**a**) – (**d**), except (**e**) – (**h**) members initialized at 0000 UTC 1 June, (**i**)–(**l**) those initialized at 0000 UTC 2 June, and (**m**)–(**p**) those initialized at 1200 UTC 2 June, respectively

some weighted ensemble may be a more balanced choice to avoid high FAs. At the two thresholds shown in Fig. 16, the above effect of EP-1 is more ideal over the mountains (BS closer to 1) than the plains as well. Overall, the QPF skill for event 2 is lower than event 1, but the rainfall over the mountains remains more predictable than the plains.

4.3 Example of ensemble rainfall probability

As another example, the probability distributions for P3 in event 2 (Fig. 17) again show that the rainfall is more predictable (with higher probabilities) in the mountains than the plains (with lower probabilities) in general, including at 130 mm at the two shorter ranges (Fig. 17k, o). Between the two rainfall areas over the plains, one in northwestern and the other in southwestern Taiwan

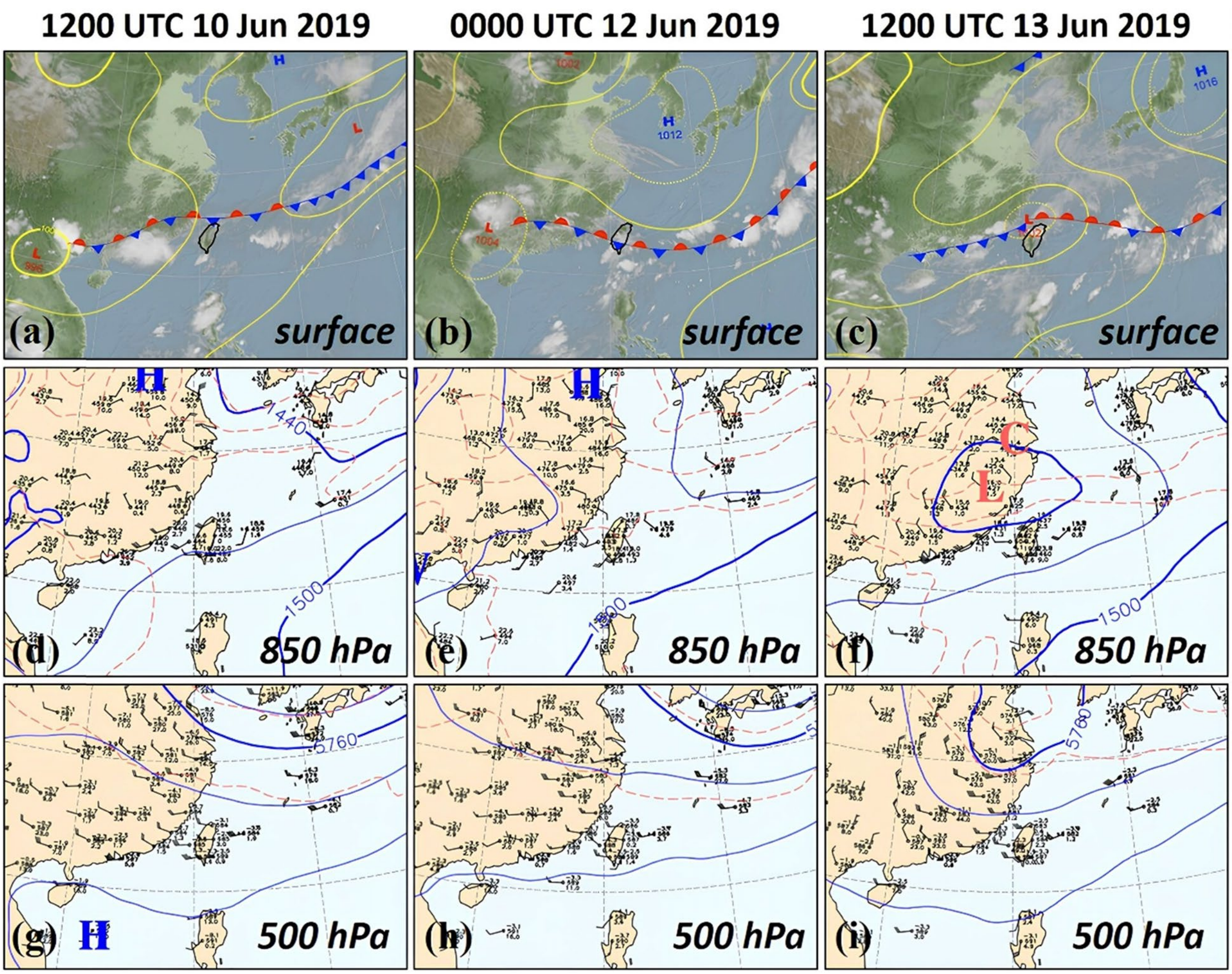

Fig. 10 As in Fig. 2, except at (**a**), (**d**), (**g**) 1200 UTC 10 June, (**b**), (**e**), (**h**) 0000 UTC 12 June, and (**c**), (**f**), (**i**) 1200 UTC 13 June 2019, respectively (as labelled), during event 2

(Fig. 12c), the former region appears to be better predicted with higher probabilities than the latter.

5 Event 3: 29 May-1 June 2021

5.1 Event overview

The third event spanned from 29 May to 1 June in 2021, as a Mei-yu front slowly moved through Taiwan from north to south (Fig. 18a – c) and then into the Bashi Channel (not shown). At 850 hPa, prevailing winds surrounding Taiwan were initially from the southwest at about 20 – 30 kts (Fig. 18d), but turning into westerlies at 1200 UTC 30 May before weakening (Fig. 18e, f) as the front advanced. Meanwhile, farther aloft at 500 hPa, a trough was passing through Taiwan with westerly flow during event 3 (Fig. 18g – i), presumably coupled with the movement of the low-level front.

Figure 19 shows the satellite IR cloud imageries at 6—h intervals during event 3, and reveals that convection was active and several MCSs developed in Taiwan and the adjacent area when the front approached and moved across Taiwan. These MCSs included the one over central and southwestern Taiwan at 0000 UTC 30 May (Fig. 19c), and a subsequent system over southwestern Taiwan during 0600 – 1200 UTC (Fig. 19d, e). Later around 1800 UTC 30 May and 0600 UTC 31 May, more convection and another MCS also developed over central CMR (Fig. 19f – h), apparently behind the front. The resultant rainfall distribution from 1200 UTC 29 May to 1200 UTC 30 May (Fig. 20a) shows widespread rainfall in central Taiwan, in both the CMR and the plain area with maxima around 220 mm, and also in southern Taiwan. Over the next 24 h from 1200 UTC 30 May to 1200 UTC 31 May, central CMR (242 mm) and the northwestern to central coastal area (peaking at 192 mm) were the main rainfall regions (Fig. 20b). The QPFs for these two periods will be verified.

5.2 Verification of QPFs

For event 3, M01 had three runs per day, with an additional one at 1800 UTC, while outputs from M04 and

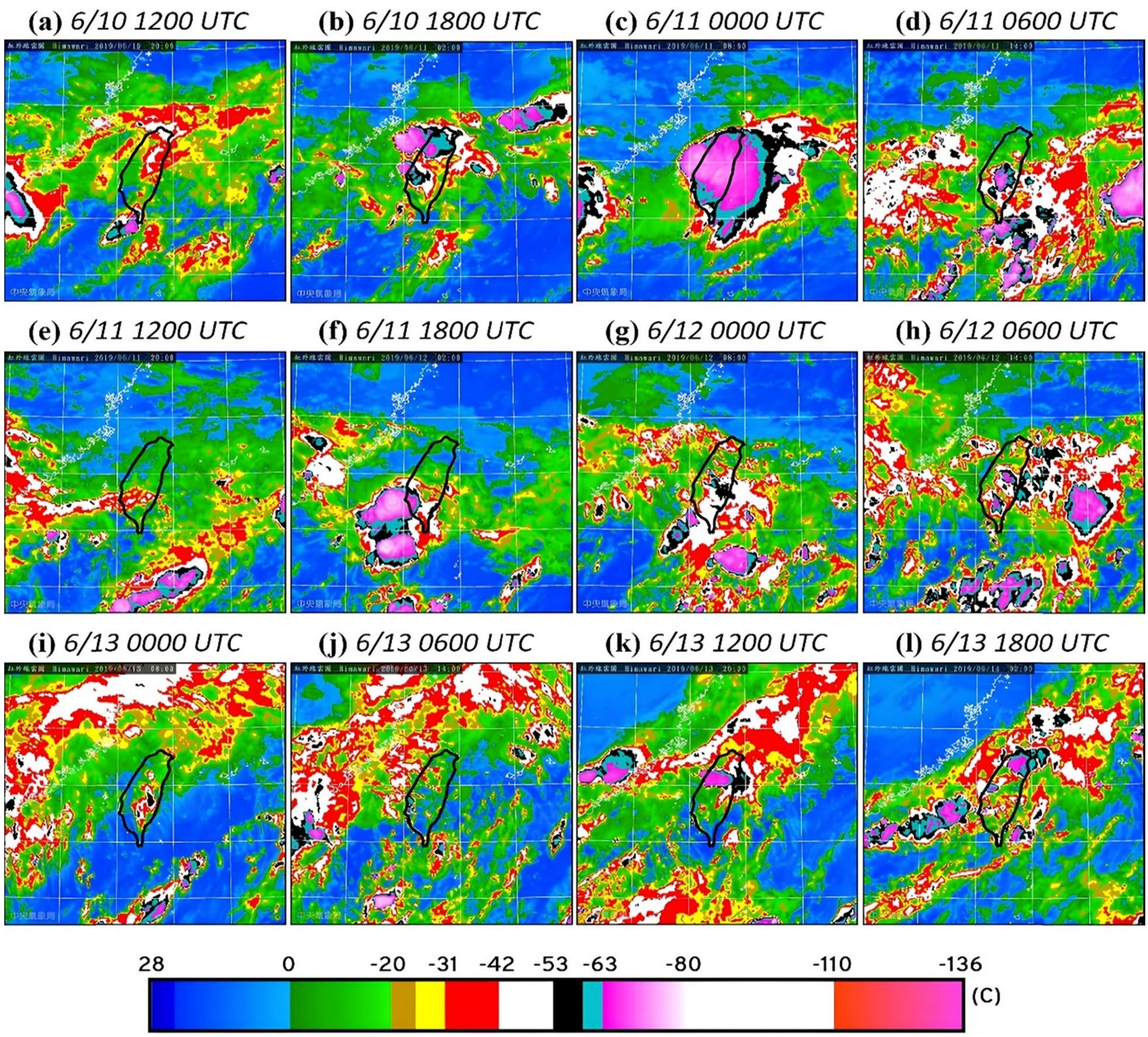

Fig. 11 As in Fig. 3, except for every 6 h from (**a**) 1200 UTC 10 June to (**h**) 0600 UTC 12 June, and then from (**i**) 0000 to (**l**) 1800 UTC 13 June 2017 during event 2

M05 were available only since 0000 UTC 30 May onward (Table 2). Figure 21 shows the overall TSs for event 3 at 50, 80, and 130 mm, integrated over the two target periods P1 and P2 (see Fig. 20). The scores at the short range for event 3 are relatively low and many members exhibit little advantage over forecasts at longer lead times. Otherwise, the overall TSs are comparable to those for event 2. At 50 – 80 mm at long ranges, M10 and M13 at times perform better. At these two thresholds, the mountain areas again tend to receive higher TSs than the plains, but such an advantage is not apparent at 130 mm, where the TSs rarely reach 0.2. At 200 mm, none of the members could produce TS > 0 except for M10 at 0 – 24 h (TS ~ 0.03), so the figure is omitted here.

In Fig. 22, the corresponding BSs at 50 and 130 mm are shown. Similar to event 2, the majority of members exhibit under-prediction even at 50 mm, and if not, their TSs are often higher. At 130 mm, the under-forecasting becomes more serious and fewer member can produce more ideal BS values. Again, the BSs are more variable and unstable over the plains than the mountains. Whenever a higher BS appears (less under-prediction or over-prediction), the TS rises due to an increased number of hits. At 200 mm, however, the BSs for event 3 (not shown) are similar to those for event 2, but all TSs remain zero as mentioned. Thus, for all three events, most members with $\Delta x \sim 3$ km still under-predict rainfall at heavy-rainfall thresholds, and a further increase in resolution appears needed.

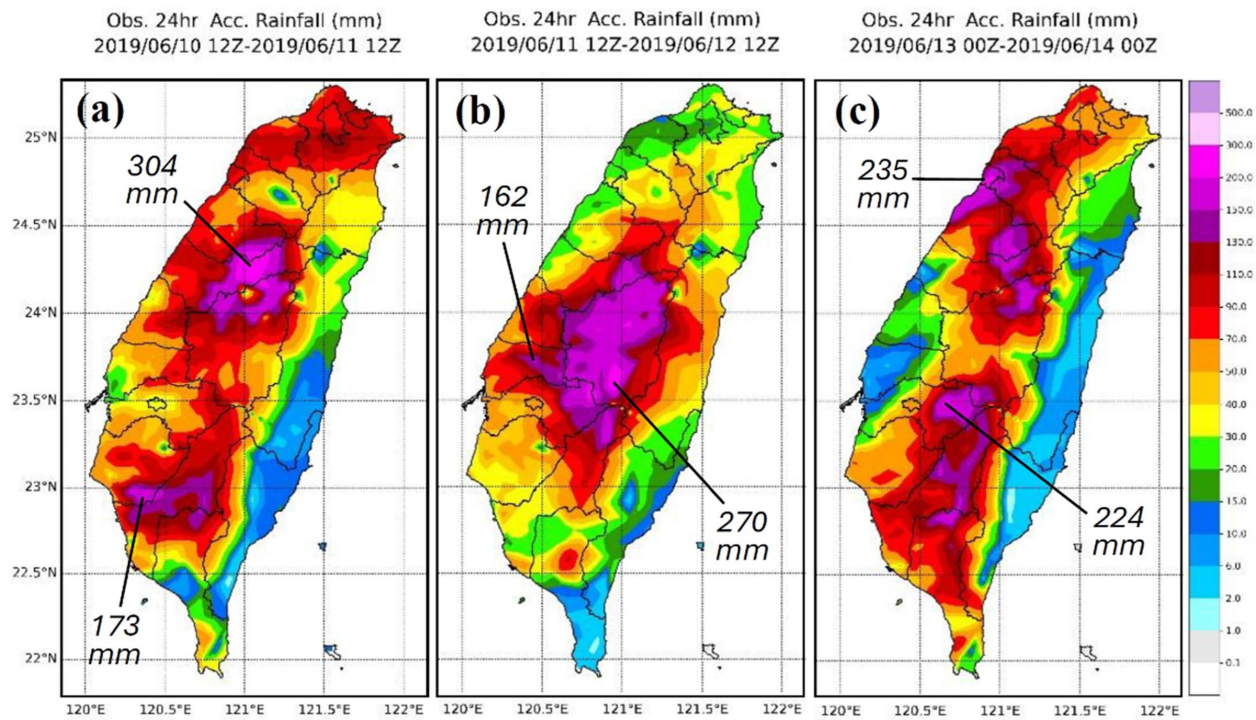

Fig. 12 As in Fig. 4, except for the 24—h period (**a**) from 1200 UTC 10 June to 1200 UTC 11 June, (**b**) from 1200 UTC 11 June to 1200 UTC 12 June, and (**c**) over 0000 – 2400 UTC 13 June 2019 during event 2, respectively

The TSs of ensemble products for event 3 are shown in Fig. 23, also at 50, 80, and 130 mm. The scores are similar to those from individual members but are more stable and consistent among products, and also higher over the mountains than the plains. The TSs show no strong variation with lead time and tend to be lower around day 4 (72 – 96 h), but the skill becomes quite limited at 130 mm. As in event 2, the EP-1 consistently has the highest TS among all products at 50 and 80 mm, mainly because it raises the BS to above 1 when individual members under-predict (see Fig. 22), especially over the plains. At 130 mm (and above), the BSs of EP-1 often become too high (figure not shown), and those of EP-2 are often more ideal, despite its TSs may be somewhat lower. For event 3, the characteristics of BSs are very similar to those for event 2, so the figure is omitted here.

6 Discussion

In this section, we focus our discussion on the first scientific goal stated in Sect. 1: Does TAHPEX show improvement in Mei-yu heavy-rainfall QPFs in Taiwan using cloud-resolving members for ensemble? To help answer this question, Table 4 is compiled from past studies and the present work to compare the TSs of 24—h QPFs at five selected thresholds of 50, 80, 130, 200, and 350 mm (per 24 h) for Mei-yu rainfall events in Taiwan since the early 2000s. Some of the past results were for the entire Mei-yu season (May – June), but the statistics at heavy-rainfall thresholds should be dominated by the larger events (see e.g., Wang et al. 2022b, 2023a). To make a fair comparison, the average skills of the members, not any of the ensemble products, are given. In the few occasions where the scores were not computed at the thresholds specified here (e.g., at 75 instead of 80 mm), linear interpolation is used to estimate the TSs. In some earlier studies, MM5 was used, while the Mei-yu results from the ensemble experiment carried out by the TTFRI in 2015 and 2016 are also adopted. Another caveat that should be noted is that these studies performed their evaluation over different Mei-yu seasons and thus different rainfall events.

From Table 4, it is clear that as the technology advances and computational resource and model resolution increase, the QPF skill at heavy-rainfall thresholds improves with time, as the later models have a grid size of at least about 3 km. Across all five thresholds and the three ranges from day 1 (0 – 24 h) to day 3 (48 – 72 h), the highest TS is either obtained by the TAHPEX or 2.5—km CReSS (same setting as M01), which span different seasons with events of different predictability. At 50, 80, and 130 mm, the TSs of TAHPEX or CReSS can reach 0.57, 0.36, and 0.22 on day 1, 0.45, 0.28, and 0.19 on day 2, and 0.34, 0.25, and 0.16 on day 3, respectively, much better than before (for days 1 – 2). Also, at 200 mm, the TSs are ≥ 0.2 at all three ranges, but the skill by 5—km models was very limited before 2016. Thus, while the TAHPEX

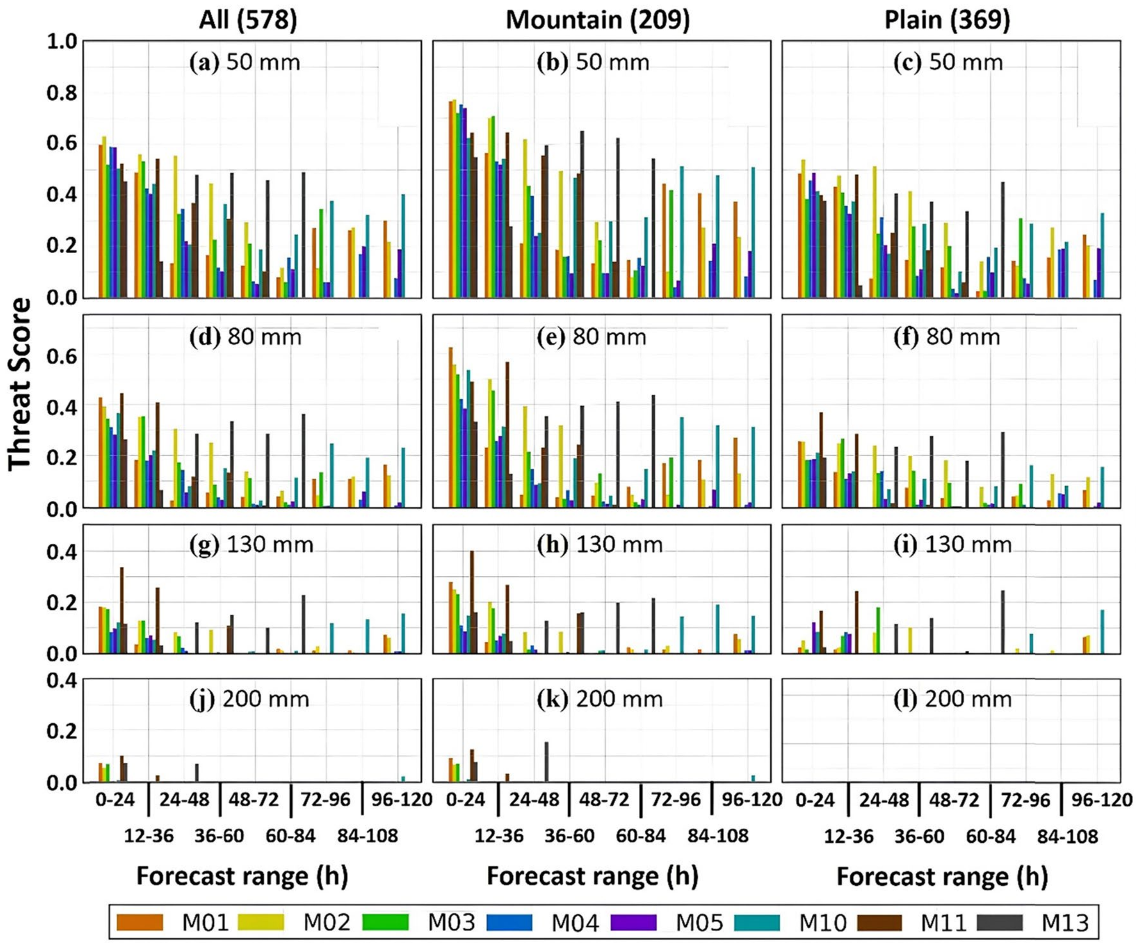

Fig. 13 As in Fig. 5, except in event 2 (combined for the three target periods) at thresholds of (**a**) – (**c**) 50 mm, (**d**) – (**f**) 80 mm, (**g**) – (**i**) 130 mm, and (**j**) – (**l**) 200 mm, respectively. The number of gauge sites were 209 over the mountains and 369 over plains, with a total of 578 sites. The forecast range is out to 96 – 120 h

members are certainly not perfect, considerable improvement has been made, not only in the TS but also in the increase in lead time. This is consistent with Wang et al. (2025b), who compared 2.5—km and 5—km CReSS with identical settings except for the grid size, over the same Mei-yu seasons of 2012 – 2014. In addition, from their once-daily runs, the 1—km TAHPEX members can quite often produce higher TSs with considerably less underprediction compared to other members, even at ranges beyond 72 h. These results suggest the potential benefits and direction for further improvement.

7 Conclusions and summary

In this study, the performance of 24—h QPFs in Mei-yu heavy-rainfall events by the cloud-resolving multi-model members and their ensemble products in the TAHPEX project during the dry-run periods is evaluated. Nine target periods from three events (1 – 4 June 2017, 10 – 14 June 2019, and 29 May – 1 June 2021) are included for verification of QPFs using skill scores such as TS and BS, at thresholds from 50 to 350 mm (per 24 h) and ranges from 0 – 24 h out to 96 – 120 h, and the ensemble products include the ensemble mean, PM, and EP from the most, second most, and third most rainy member (EP-1, EP-2, and EP-3), respectively. Various aspects of the results are discussed, including the performance against past results, the contrasting QPF skills over the mountains compared to the plain regions of Taiwan, the usefulness of ensemble products, and the QPFs by the 1—km members with a finer grid. The major findings are summarized below.

First, compared to past evaluations on 5—km models, TAHPEX members show significant improvement in TS at heavy-rainfall thresholds and also in lead time. At 130 mm, for example, they exhibit a TS of over 0.2 on day 1, and not much lower on day 2 (0.19) and day 3 (0.15). At 200 mm, the TSs are only slightly lower as well. At 350 mm, however, the TS are ≤ 0.1 in general, suggesting only limited skill at such a high threshold. From the limited number of forecasts by the two 1—km members,

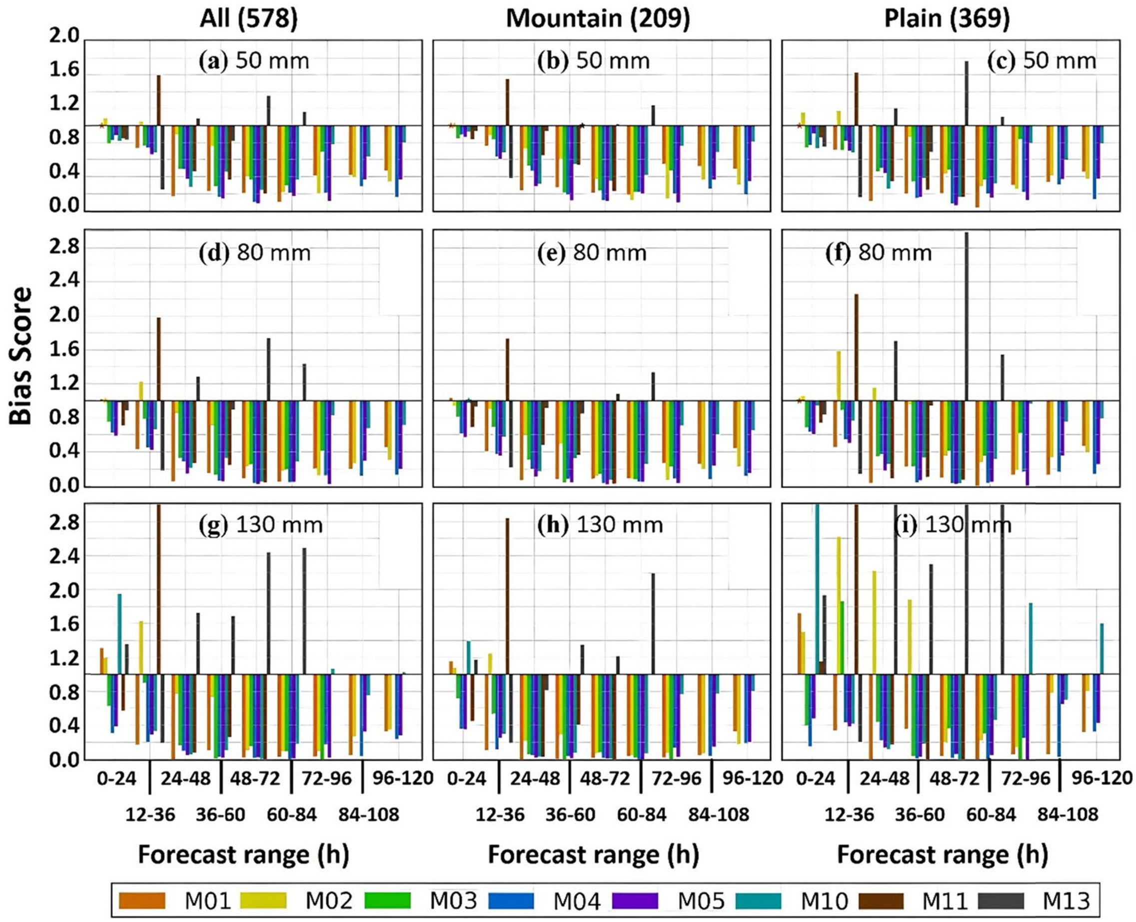

Fig. 14 As in Fig. 13, except showing the BS values in event 2 at (**a**) – (**c**) 50 mm, (**d**) – (**f**) 80 mm, and (**g**) – (**i**) 130 mm, respectively

they show potential for further improvement both over mountains and plains.

Second, the BS values indicate under-prediction over heavy-rainfall thresholds by most members even with convective-permitting capabilities, more serious toward higher thresholds and ranges around 48 – 72 h and longer, except at 80 mm and below in event 1. Such under-forecast is overall less severe in the mountains (elevation > 300 m) compared to the plains (elevation ≤ 300 m). At the same time, a few members can over-predict, but tend to produce only misses and FAs with very few hits. Such a scenario is also more serious toward high thresholds and over the plains. Given the results of mostly under-prediction at Δx of 2.5 – 3 km, a further increase in model resolution seems beneficial but this remains to be confirmed.

Third, the Mei-yu rainfall over the mountains in Taiwan exhibits significantly higher predictability than rainfall over the plains. This is reflected in consistently higher TS values, more stable and smaller ranges of variation in BS (less serious over- and under-prediction), and higher heavy-rainfall probabilities by the ensemble across nearly all thresholds and all forecast ranges, in all three events. This finding has significant implications, as heavy-rainfall events in Taiwan occur more frequently in the mountains, where they are phase-locked and more predictable compared to those over the plains from transient systems.

Fourth, derived from 3 – 10 runs, the five ensemble products perform more stably in QPFs than individual members and thus are useful: the EP-1, with largest rain areas, consistently exhibits the highest TS among all products, except at 50—80 mm and the short range within 12 – 36 h in events 1 and 2. Because the best member is not known in advance, the certainty of EP-1 makes it useful in routine operation. However, the better TS of EP-1 than other products is at the expense of excessive BS, especially over the plains, so other products may offer a more balanced choice.

Some other results are also worth mentioning. The overall skill of QPFs is higher in the 2017 event, which was a larger rainfall event in magnitude, consistent with Wang (2015) and Wang et al. (2021b, 2022b). On the other hand, the spin-up issue at the shortest range also appears more significant in this more extreme event. Among the ensemble products, the TSs of PM and EP-2

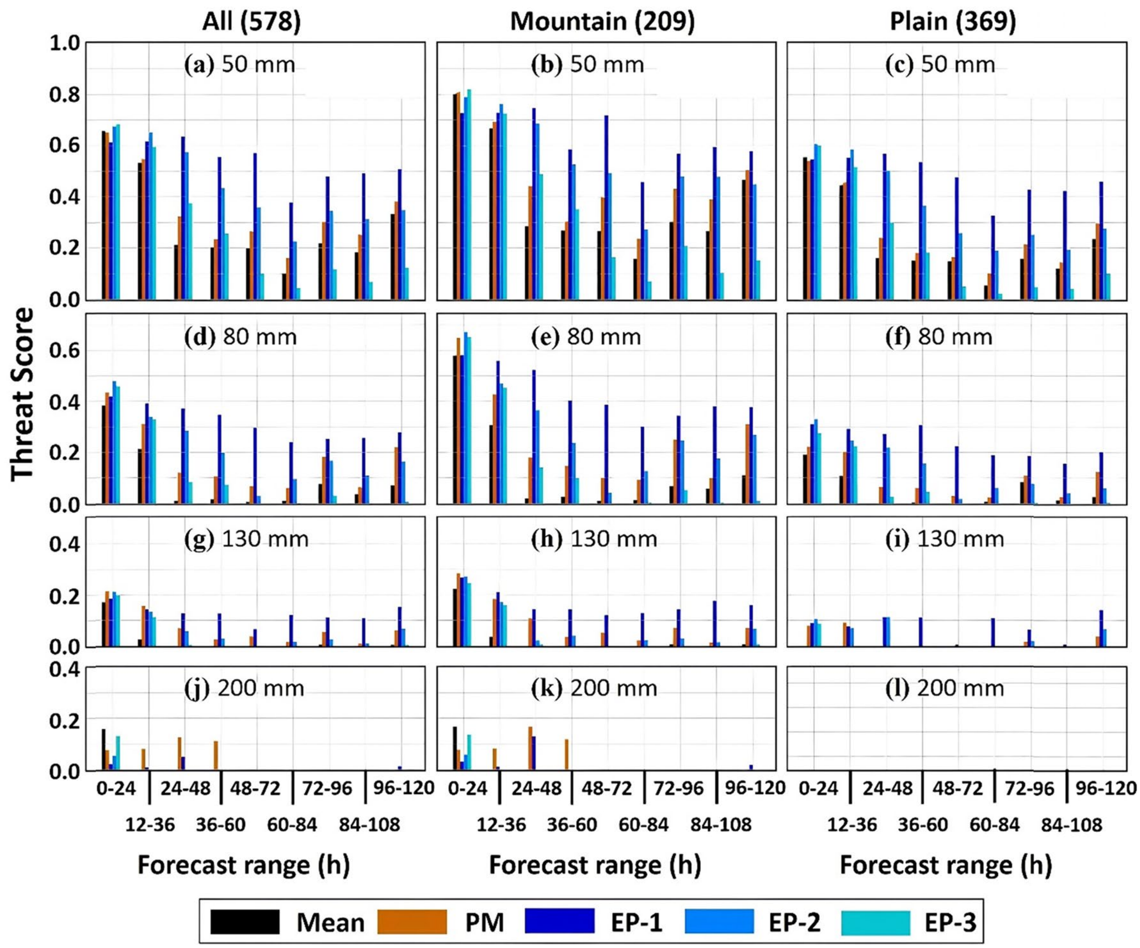

Fig. 15 As in Fig. 13, except showing the TS values of ensemble products in event 3

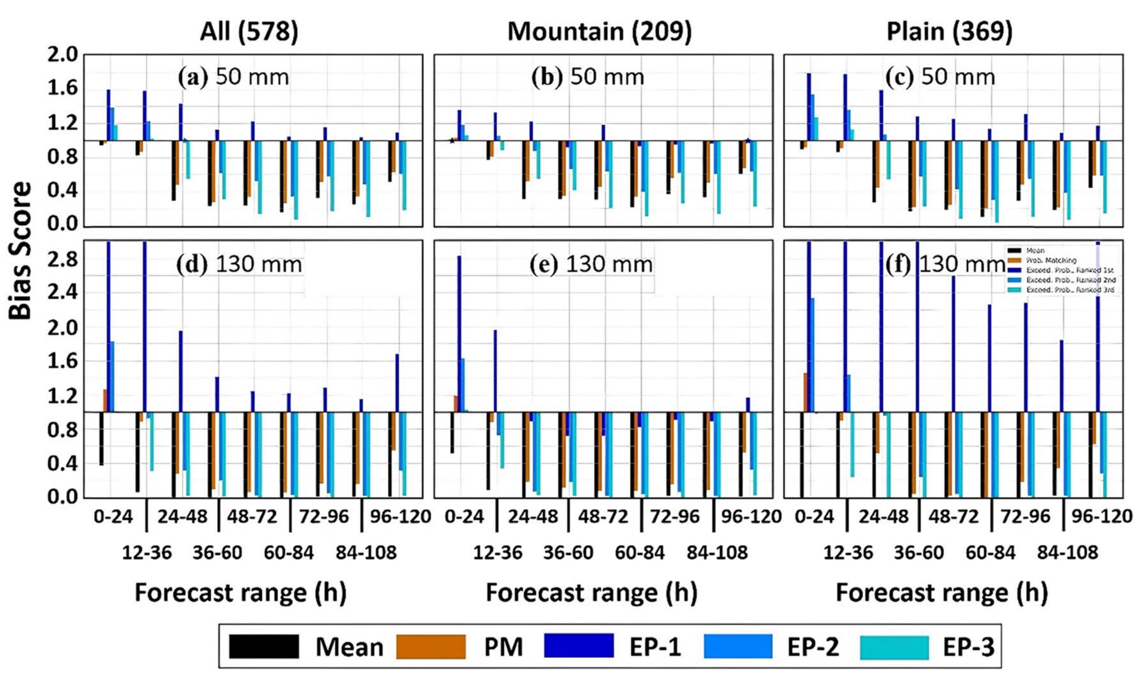

Fig. 16 As in Fig. 15, except showing the BS values in event 3 at (**a**) – (**c**) 50 mm and (**d**) – (**f**) 130 mm, respectively

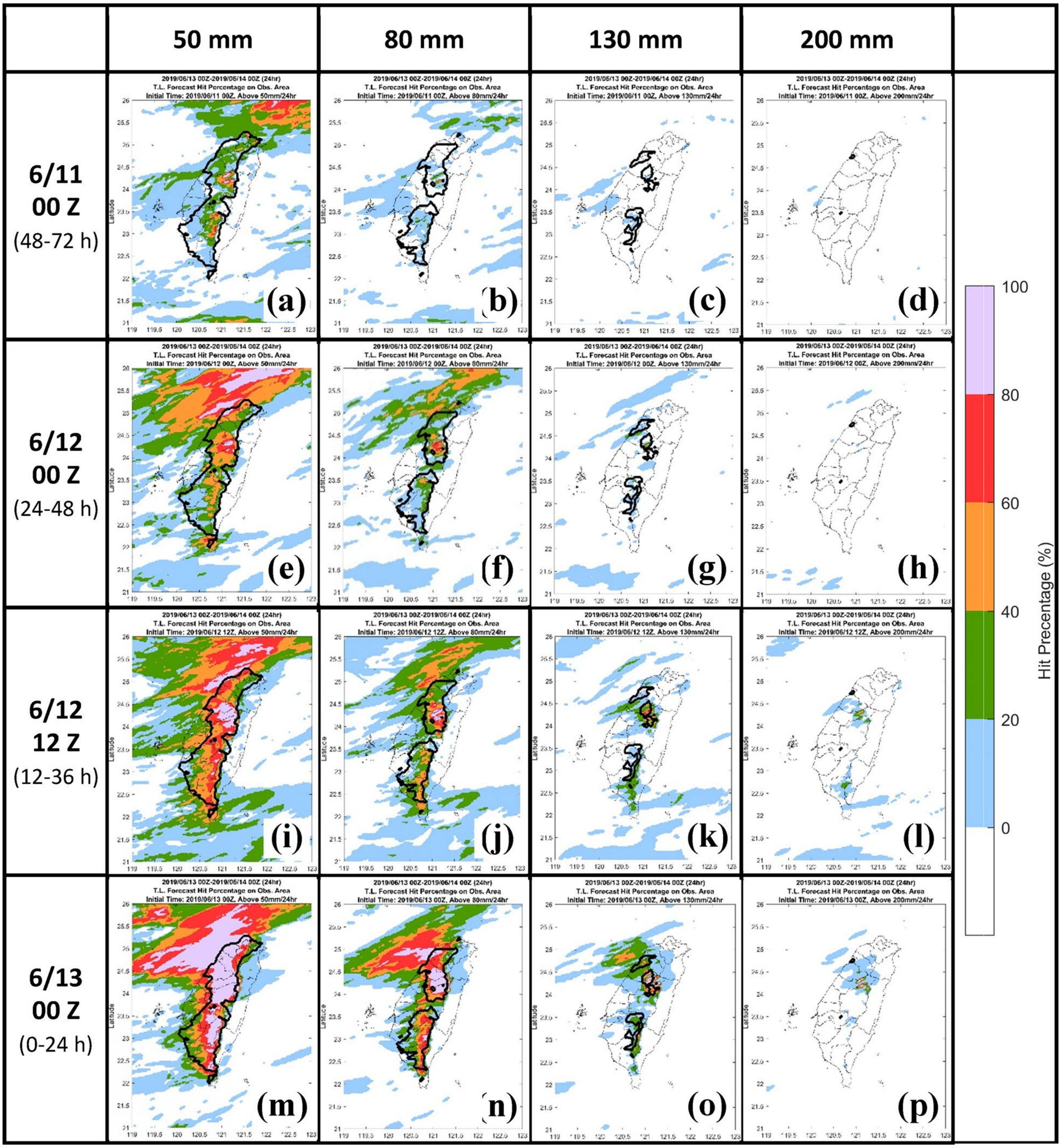

Fig. 17 As in Fig. 9, except showing the probabilities of 24—h QPFs (%) from members initialized at the time labelled to reach 50, 80, 130, and 200 mm, respectively, for target period 3 in event 2 (0000 UTC 13 June to 0000 UTC 14 June 2019)

are often comparable (but lower than EP-1), followed by EP-3 and the ensemble mean, which under-estimates the peak values of rainfall as expected. In conclusion, the higher predictability of heavy rainfall over the mountains than the plains in Taiwan suggests that their QPFs need to be perceived and applied differently to maximize their usefulness in hazard reduction. More studies to further explore these aspects in greater depth are also recommended in the near future.

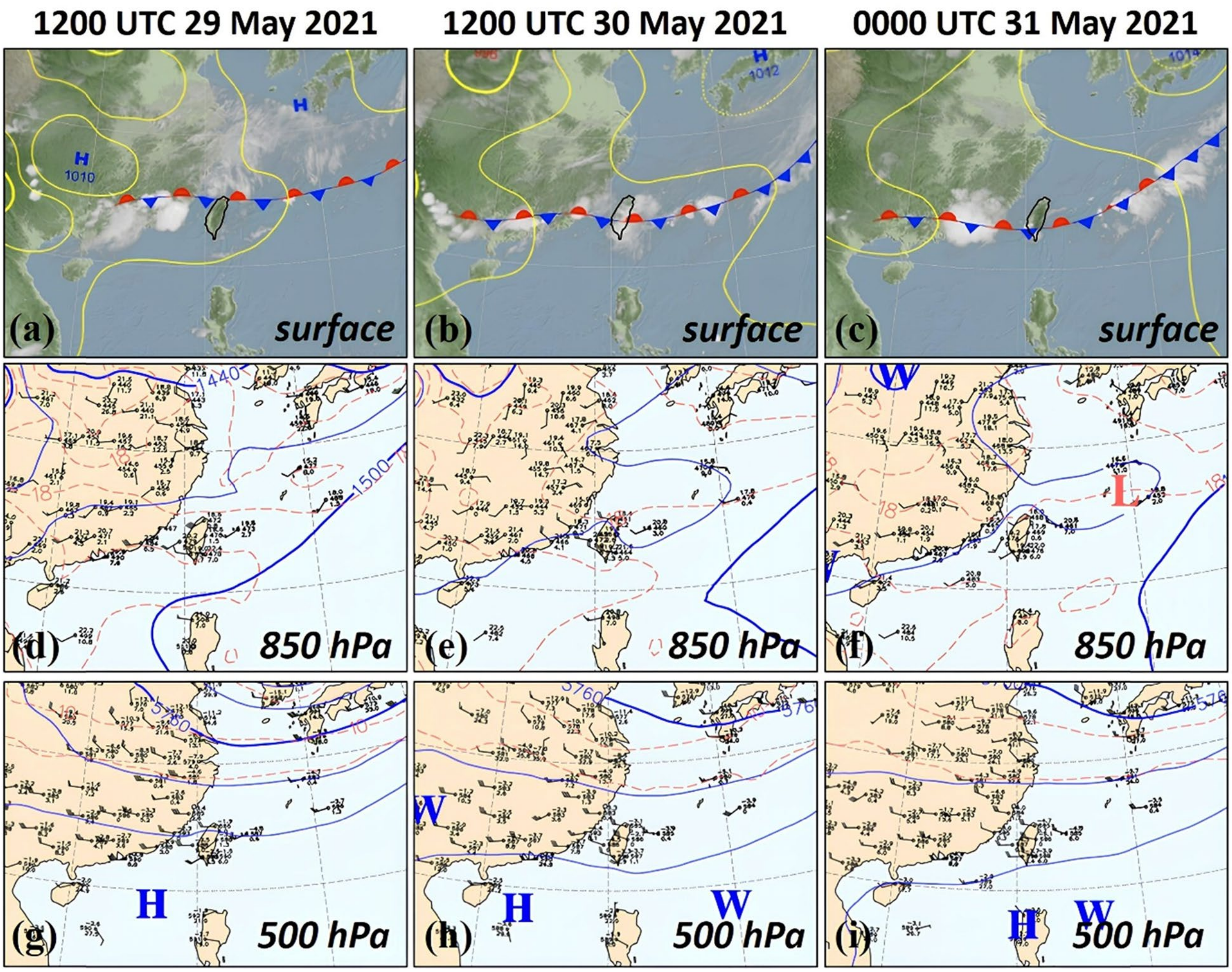

Fig. 18 As in Fig. 2, except at (**a**),(**d**),(**g**) 1200 UTC 29 May, (**b**), (**e**), (**h**) 1200 UTC 30 May, and (**c**), (**f**), (**i**) 0000 UTC 31 May 2021, respectively (as labelled), during event 3

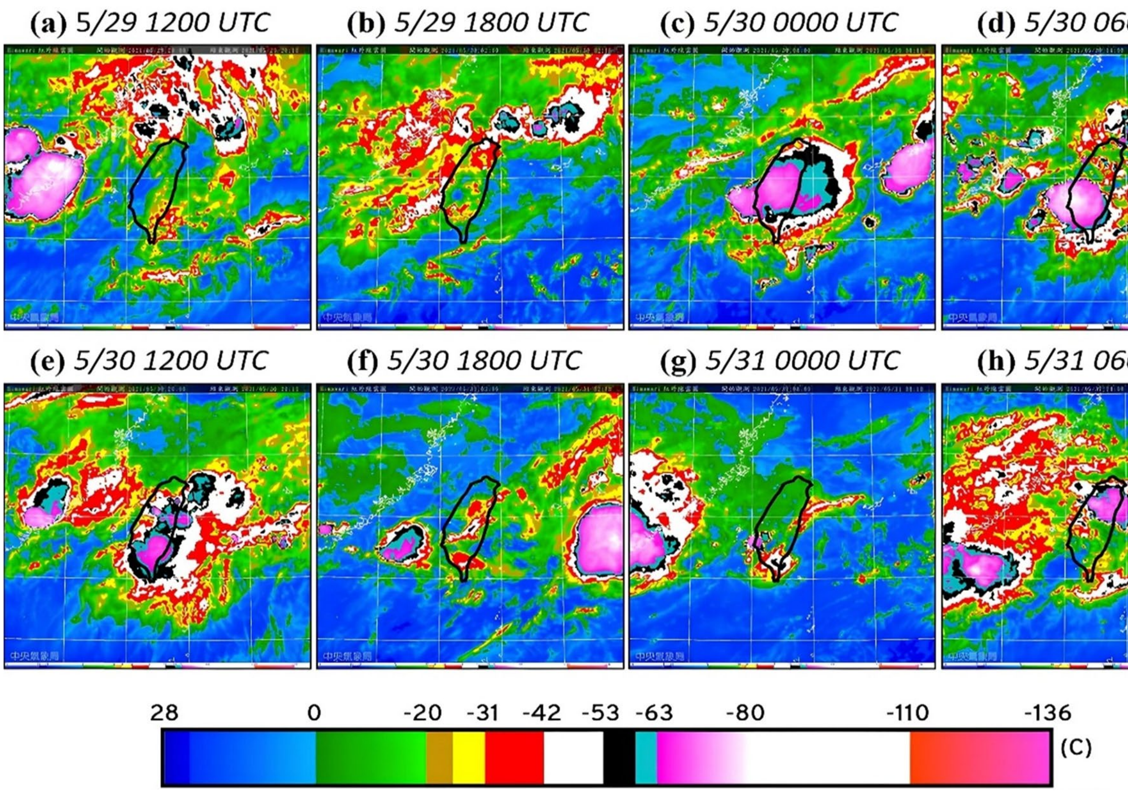

Fig. 19 As in Fig. 3, except for every 6 h from (**a**) 1200 UTC 29 May to (**h**) 0600 UTC 31 May 2021 during event 3

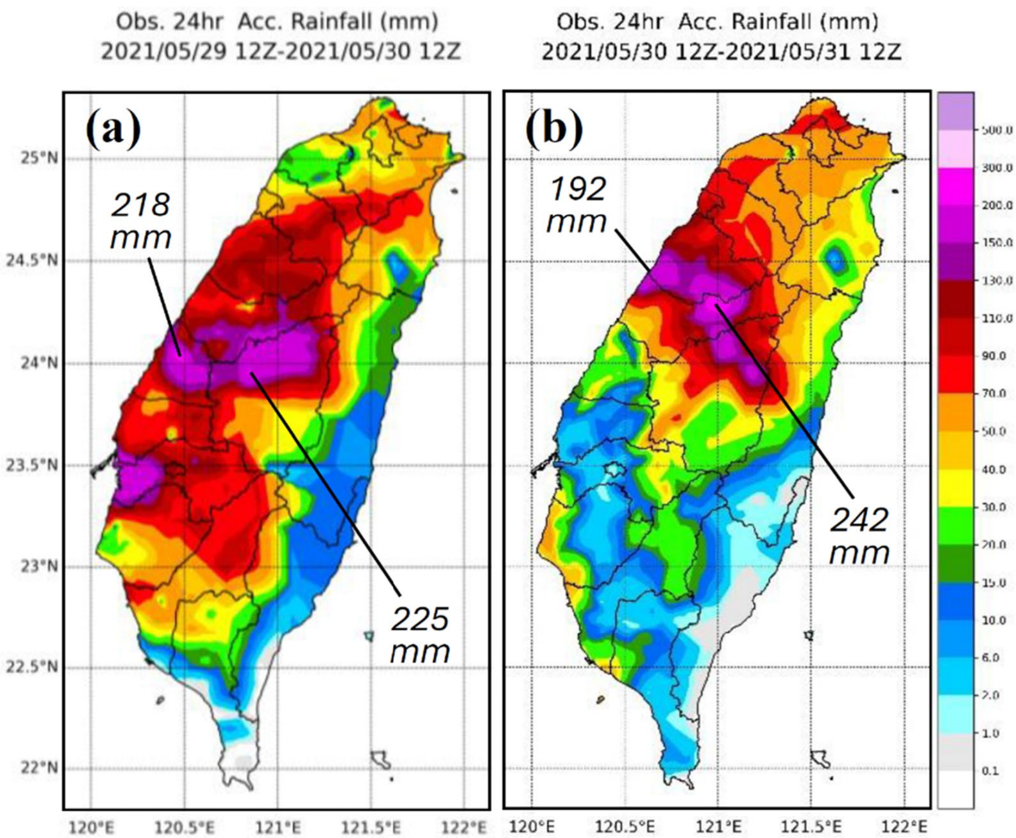

Fig. 20 As in Fig. 4, except for the 24—h period (**a**) from 1200 UTC 29 May to 1200 UTC 30 May, and (**b**) from 1200 UTC 30 May to 1200 UTC 31 May 2021 during event 3, respectively

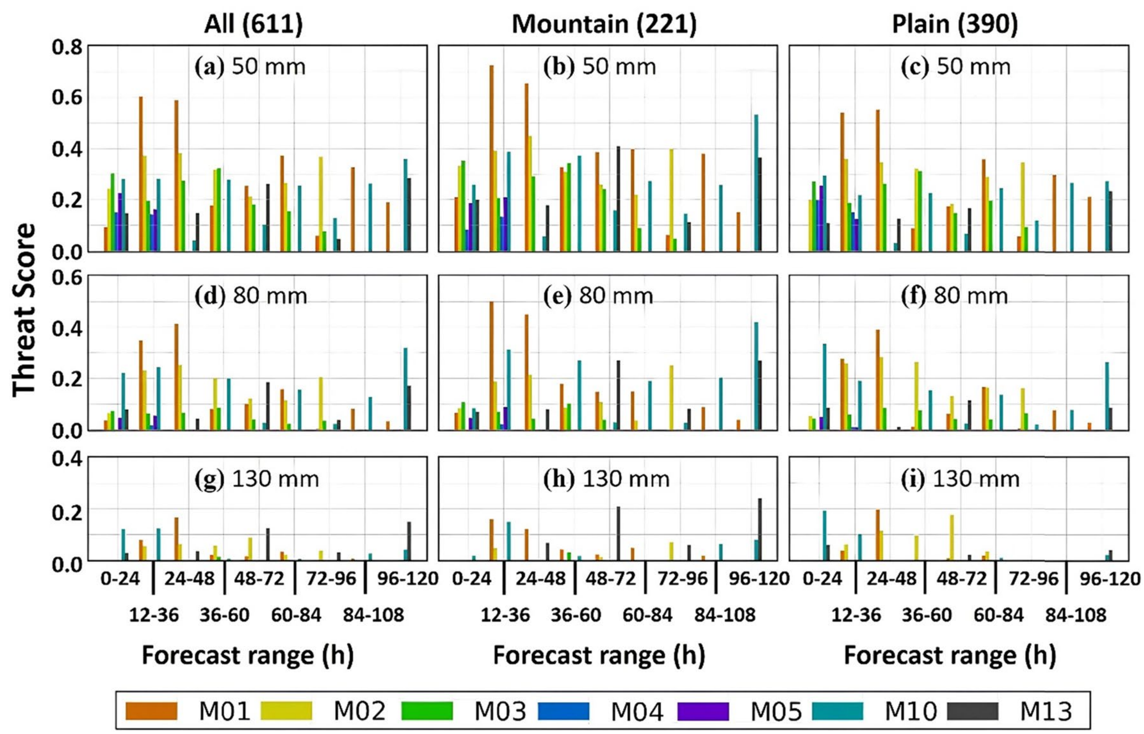

Fig. 21 As in (**a**) – (**i**) of Fig. 13, except for event 3, combined for the two target periods. The number of gauge sites were 221 over the mountains and 390 over plains, with a total of 611 sites

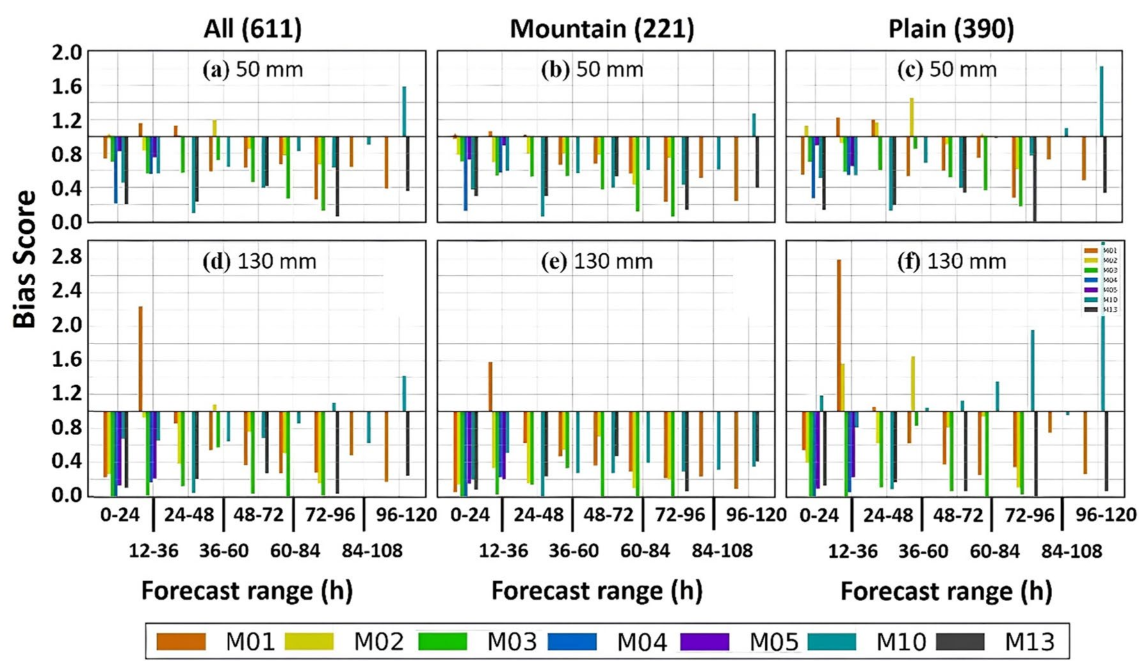

Fig. 22 As in Fig. 21, except showing the BS values in event 3 at (**a**) – (**c**) 50 mm and (**d**) – (**f**) 130 mm, respectively

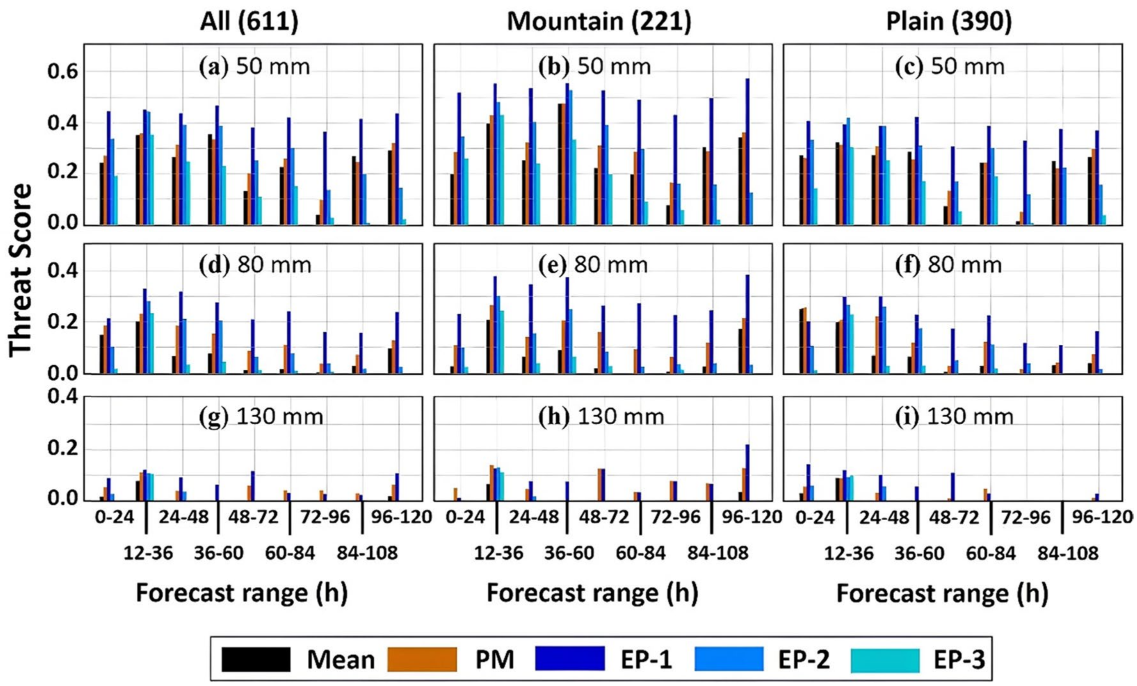

Fig. 23 As in Fig. 21, except showing the TS values of ensemble products in event 3

Table 4 Comparison of TS values of 24—h QPFs at fixed thresholds over 50 – 350 mm in Taiwan Mei-yu season by major efforts or studies since the early 2000s leading to TAHPEX. Some values are estimated using averaging or linear interpolation and/or given a range, and the dash "–" means that no verification is available at that threshold and range. The highest value over the years is highlighted in bold face

Forecast range	Rainfall threshold (mm)	Before 2012 5—km MM5/WRF[a]	2013 – 14 CWA 5—km WRF[b]	2015 – 16 TTFRI 5—km models[c]	2012 – 17 2.5—km CReSS[d]	2017 – 21 TAHPEX members
Day 1 (0—24 h)	50	≤ 0.11	< 0.14 – 0.17	~ 0.40	0.40	**0.57**
	80	–	< 0.09 – 0.12	~ 0.31	0.29	**0.36**
	130	–	< 0.05	0.16 – 0.22	0.21	**0.22**
	200	–	< 0.02	0.03 – 0.09	0.15	0.10 – **0.31**
	350	–	0.00	≤ 0.01	**0.11**	< 0.04
Day 2 (24—48 h)	50	–	< 0.07 – 0.11	–	0.36	**0.45**
	80	–	< 0.07 – 0.09	–	0.27	**0.28**
	130	–	< 0.07	–	**0.19**	0.17
	200	–	< 0.02	–	0.16	0.13 – **0.26**
	350	–	0.00	–	0.03	0.02 – **0.08**
Day 3 (48—72 h)	50	–	–	–	**0.34**	0.31
	80	–	–	–	**0.25**	0.22
	130	–	–	–	**0.16**	0.15
	200	–	–	–	0.10	0.06 – **0.23**
	350	–	–	–	0.03	< **0.05**

[a] Taken from Wang et al. (2017) and references cited in Wang et al. (2022a); [b] From Fig. 2 of Wang et al. (2022a); [c] From TTFRI annual reports (in Chinese), targeted for major Mei-yu events, at range of 6 – 36 h; [d] From Wang et al. (2023a), an update from Wang et al. (2022a) through the 2012 – 2017 Mei-yu seasons, for group A (minor events excluded)

Abbreviations

BS Bias score
CReSS Cloud-Resolving Storm Simulator
CMR Central Mountain Range
CWA Central Weather Administration
DA Data assimilation
EP Exceedance probability
FA False alarm
GFDL Geophysical Fluid Dynamics Laboratory
GFS Global Forecast System
IC/BC Initial and boundary condition
IR Infrared
MCS Mesoscale convective systems
MM5 Mesoscale Model version 5
MRF Medium-Range Forecast
NCEP National Centers for Environmental Prediction

PBL	Planetary boundary layer
PM	Probability matching
QPF	Quantitative precipitation forecast
SUM	Spectral Unified Model
TAHOPE	Taiwan Area Heavy rain observation and Prediction Experiment
TAHPEX	Taiwan Area Heavy-rainfall Prediction Experiment
TGFS	Taiwan Global Forecast System
TKE-EDMF	Turbulent kinetic energy-based moist eddy-diffusion mass-flux
TS	Threat score
TTFRI	Taiwan TyphoonG and Flood Research Institute
TWRF	Typhoon WRF
WDM6	WRF double-moment 6 class
WRF	Weather Research and Forecasting
WRF-D	Deterministic WRF
WSM3	WRF single-moment 3 class
YSU	Yonsei University

Supplementary Information

The online version contains supplementary material available at https://doi.org/10.1007/s44195-026-00132-1.

Supplementary file1

Acknowledgements

We thank the contributions from TAHPEX team and participants not included in the authors' list. The NCEP is acknowledged for providing real-time GFS data that drive most of the TAHPEX members, and the CWA for providing the observation and rainfall data. The official name of the CWA was the Central Weather Bureau (CWB) prior to September 2023.

Author contributions

Chung-Chieh Wang: conceptualization, funding acquisition, supervision, experiment design, methodology, data analysis, investigation and validation, visualization, discussion, writing draft, review and editing. Po-Yu Huang: methodology, data analysis, investigation and validation, software, visualization, discussion, writing draft. Jing-Shan Hong: data curation, data consultation. Fang-Ching Chien, Ming-Jen Yang, Ling-Feng Hsiao, Chien-Her Chen, Chih-Sheng Chang, Pay-Liam Lin, Rosimar Rios-Berrios, Ching-Yuang Huang, Bill Skamarock, Bo-Xun Lin, and Guo-Yuan Lien: data curation. Shin-Hau Chen: data curation, software. Pi-Yu Chuang, Cheng-Chin Liu, Shin-Yi Huang, and Yi-Wen Wang: software. Guo-Chen Leu and Chin-Tzu Fong: funding acquisition, supervision. All authors: review and editing.

Funding

Open access funding provided by National Taiwan Normal University. This study was supported by the National Science and Technology Council (NSTC) of Taiwan, jointly under grants MOST 108—2111-M-003—005-MY2, MOST 110—2111-M-003—004, MOST 111—2111-M-003—005, NSTC 112—2111-M-003—005, NSTC 113—2111-M-003—001, and NSTC 114—2111-M-003—004.

Data availability

The QPF data utilized in this study are available from the TAHPEX project upon request. The various models participating in TAHPEX are available for download from their websites. The NCEP GFS data are available at http://rda.ucar.edu/datasets/ds335.0/#!description. The observation data are available from the CWA (https://www.cwa.gov.tw/eng/) upon request.

Declarations

Ethics approval and consent to participate

Not applicable.

Consent for publication

Not applicable.

Competing interests

The authors declare no competing interests.

Author details

[1]Department of Earth Sciences, National Taiwan Normal University, No. 88, Sec. 4, Ting-Chou Rd., Taipei 11677, Taiwan
[2]Central Weather Administration, No. 64, Gongyuan Rd., Taipei 100006, Taiwan
[3]Department of Atmospheric Sciences, National Taiwan University, No. 1, Sec. 4, Roosevelt Rd., Taipei 106319, Taiwan
[4]Department of Atmospheric Sciences, National Central University, No. 300, Jung-da Rd., Jhung-Li 320, Taoyuan, Taiwan
[5]National Center for Atmospheric Research, P.O. Box 3000, Boulder, CO 80307-3000, USA

Received: 26 January 2026 / Accepted: 30 April 2026
Published online: 05 August 2026

References

Braun SA (2002) A cloud-resolving simulation of Hurricane Bob (1991): storm structure and eyewall buoyancy. Mon Weather Rev 130:1573–1592
Chang CP, Yang YT, Kuo HC (2013) Large increasing trend of tropical cyclone rainfall in Taiwan and the roles of terrain. J Clim 26:4138–4147
Chen YH, Sha SH, Lin CH, Hsiao LF, Huang CY, Kuo HC (2024) Performance evaluation of TGFS typhoon track forecasts over the western North Pacific with sensitivity tests on cumulus parameterization. Atmosphere Basel 15:1075. https://doi.org/10.3390/atmos15091075
Chi SS (2006) The Mei-Yu in Taiwan. SFRDEST E-06-MT-03–4, Chung-Shin Engineering Technology Research and Development Foundation, Taipei, Taiwan, p 65 (in Chinese)
Chien FC, Kuo HC (2011) On the extreme rainfall of Typhoon Morakot (2009). J Geophys Res 116:D05104
Chien FC, Liu YC, Lee CS (2008) Heavy rainfall and southerly flow after the leaving of Typhoon Mindulle (2004) from Taiwan. J Meteorol Soc Jpn 86:17–44
Clark AJ, Gallus WA, Xue M, Kong F (2009) A comparison of precipitation forecast skill between small convection-allowing and large convection-parameterizing ensembles. Wea Forecast 24:1121–1140. https://doi.org/10.1016/S0022-1694(00)00343-7
Cuo L, Pagano TC, Wang Q (2011) A review of quantitative precipitation forecasts and their use in short- to medium-range streamflow forecasting. J Hydrometeorol 12:713–728
Davis CA, Lee WC (2012) Mesoscale analysis of heavy rainfall episodes from SoWMEX/TiMREX. J Atmos Sci 69:521–537
Davis CA, Brown B, Bullock R (2006) Object-based verification of precipitation forecasts. Part I: Methodology and application to mesoscale rain areas. Mon Weather Rev 134:1772–1784
Deardorff JW (1980) Stratocumulus-capped mixed layers derived from a three-dimensional model. Bound-Layer Meteorol 18:495–527
Done J, Davis CA, Weisman M (2004) The next generation of NWP: explicit forecasts of convection using the Weather Research and Forecasting (WRF) model. Atmos Sci Lett 5:110–117. https://doi.org/10.1002/asl.72
Dudhia J (2005) MM5 Version 3.7 (The Final Version). WRF/MM5 Users' Workshop, June 2005. National Center for Atmospheric Research. Boulder, Colorado, USA
Ebert EE (2001) Ability of a poor man's ensemble to predict the probability and distribution of precipitation. Mon Weather Rev 129:2461–2480. https://doi.org/10.1016/S0022-1694(00)00343-7
Ebert EE, McBride JL (2000) Verification of precipitation in weather systems: determination of systematic errors. J Hydrol 239:179–202. https://doi.org/10.1016/S0022-1694(00)00343-7
Ebert EE, Damrath U, Wergen W, Baldwin ME (2003) The WGNE assessment of short-term quantitative precipitation forecasts (QPFs) from operational numerical weather prediction models. Bull Am Meteorol Soc 84:481–492
Eckel FA, Mass CF (2005) Aspects of effective mesoscale, short-range ensemble forecasting. Wea Forecast 20:328–350
Epstein ES (1969) Stochastic dynamic prediction. Tellus 21:739–759
Fang X, Kuo YH (2013) Improving ensemble-based quantitative precipitation forecasts for topography-enhanced typhoon heavy rainfall over Taiwan with a modified probability-matching technique. Mon Weather Rev 141:3908–3932. https://doi.org/10.1175/MWR-D-13-00012.1
Fang X, Kou YH, Wang A (2011) The impact of Taiwan topography on the predictability of Typhoon Morakot's record-breaking rainfall: a high-resolution ensemble simulation. Wea Forecast 26:613–633. https://doi.org/10.1175/WAF-D-10-05020.1

Fawcett L, Walshaw D (2013) Estimating the probability of simultaneous rainfall extremes within a region: a spatial approach. J Appl Stat. https://doi.org/10.1080/02664763.2013.856872
Fritsch JM, Carbone RE (2004) Improving quantitative precipitation forecasts in the warm season: a USWRP research and development strategy. Bull Am Meteorol Soc 85:955–966
Gentry MS, Lackmann GM (2010) Sensitivity of simulated tropical cyclone structure and intensity to horizontal resolution. Mon Weather Rev 138:688–704
Grell GA, Dudhia J, Stauffer DR (1994) A description of the fifth generation Penn State/NCAR mesoscale model (MM5) NCAR Tech. Note NCAR/TN-3981STR Boulder. Colorado, USA
Hohenegger C, Schär C (2007) Atmospheric predictability at synoptic versus cloud-resolving scales. Bull Am Meteorol Soc 88:1783–1793
Hong JS, Fong CT, Hsiao LF, Yu YC, Tzeng CY (2015) Ensemble typhoon quantitative precipitation forecasts model in Taiwan. Weather Forecast 30:217–237
Hsiao LF, Yang MJ, Lee CS, Kuo HC, Shih DS, Tsai CC, Wang CJ, Chang LY, Chen DYC, Feng L, Hong JS, Fong CT, Chen DS, Yeh TC, Huang CY, Guo WD, Lin GF (2013) Ensemble forecasting of typhoon rainfall and floods over a mountainous watershed in Taiwan. J Hydrol 506:55–68. https://doi.org/10.1016/j.jhydrol.2013.08.046
Hsiao LF, Huang XY, Kuo YH, Chen DS, Wang H, Tsai CC, Yeh TC, Hong JS, Fong CT, Lee CS (2015) Blending of global and regional analyses with a spatial filter: application to typhoon prediction over the western North Pacific Ocean. Weather Forecast 30:754–770. https://doi.org/10.1175/WAF-D-14-00047.1
Hsiao LF, Chen DS, Hong JS, Yeh TC, Fong CT (2020) Improvement of the numerical tropical cyclone prediction system at the Central Weather Bureau of Taiwan: TWRF (typhoon WRF). Atmosphere Basel 11:657. https://doi.org/10.3390/atmos11060657
Hsu J (1998) ARMTS up and running in Taiwan. Vaisala News 146:24–26
Hsu HH, Kuo HC, Jou JD, Chen TC, Lin PH, Yeh TC, Wu CC (2010) Scientific report on Typhoon Morakot (2009). National Science Council, Taiwan, p 192 (in Chinese)
Jolliffe IT, Stephenson DB (2003) Forecast Verification: A Practitioner's Guide in Atmospheric Science. Wiley and Sons, Hoboken, NY, USA
Jou BJD, Lee WC, Johnson RH (2011) An overview of SoWMEX/TiMREX. In: Chang CP, Ding Y, Lau NC, Johnson RH, Wang B, Yasunari T (eds) The global monsoon system: research and forecast, 2nd ed. World Scientific, Singapore, pp 303–318. https://doi.org/10.1142/9789814343411_0018
Kuo YH, Chen GTJ (1990) The Taiwan Area Mesoscale Experiment (TAMEX): an overview. Bull Am Meteorol Soc 71:488–503. https://doi.org/10.1175/1520-0477(1990)071%3c0488:TTAMEA%3e2.0.CO;2
Lin CH, Lien GY, Hsiao LF (2026) Evaluating modifications to Tiedtke cumulus parameterization for improving summer precipitation forecasts in the nested grid of Taiwan Global Forecast System (TGFS v1.1). EGUsphere (preprint). https://doi.org/10.5194/egusphere-2025-5324
Liu Y, Zhang DL, Yau MK (1999) A multiscale numerical study of Hurricane Andrew (1992). Part II: kinematics and inner-core structures. Mon Weather Rev 127:2597–2616
Lorenz EN (1963) Deterministic nonperiodic flow. J Atmos Sci 20:130–141
Lu C, Yuan H, Schwartz BE, Benjamin S (2007) Short-range numerical weather prediction using time-lagged ensembles. Wea Forecast 22:580–595
Mittermaier MP (2007) Improving short-range high-resolution model precipitation forecast skill using time-lagged ensembles. Q J R Meteorol Soc 133:1487–1500
Mullen SL, Buizza R (2001) Quantitative precipitation forecasts over the United States by the ECMWF ensemble prediction system. Mon Wea Rev 129:638–663
Powers JG, Klemp JB, Skamarock WC, Davis CA, Dudhia J, Gill DO et al (2017) The weather research and forecasting model: overview, system efforts, and future directions. Bull Am Meteorol Soc 98:1717–1737. https://doi.org/10.1175/BAMS-D-15-00308
Schaefer JT (1990) The critical success index as an indicator of warning skill. Wea Forecast 5:570–575
Shen BW, Pielke RA, Zeng X, Baik JJ, Faghih-Naini S, Cui J, Atlas R (2021) Is weather chaotic? Coexistence of chaos and order within a generalized Lorenz model. Bull Am Meteorol Soc 102:E148–E158
Skamarock WC, Klemp JB, Dudhia J, Gill DO, Barker DM, Wang W, Powers JG (2005) A description of the Advanced Research WRF version 2. National Center for Atmospheric Reasearch, Boulder, Colorado, USA. https://doi.org/10.5065/D6DZ069T
Su SH, Kuo HC, Hsu LH, Yang YT (2012) Temporal and spatial characteristics of typhoon extreme rainfall in Taiwan. J Meteorol Soc Jpn 90:721–736
Toth Z, Kalnay E (1993) Ensemble forecasting at NMC: the generation of perturbations. Bull Am Meteorol Soc 74:2317–2330
Trilaksono NJ, Otsuka S, Yoden S (2012) A time-lagged ensemble simulation on the modulation of precipitation over West Java in January–February 2007. Mon Wea Rev 140:601–616. https://doi.org/10.1175/MWR-D-11-00094.1
Tsuboki K, Sakakibara A (2002) Large-scale parallel computing of cloud resolving storm simulator. In: High performance computing. Zima HP et al. (ed) 4th International Symposium. Lecture notes in computer science, Springer, Berlin, Germany, 2327; 243–259
Tsuboki K, Sakakibara A (2007) Numerical prediction of high-impact weather systems: The textbook for the seventeenth IHP training course in 2007. Hydrospheric Atmospheric Research Center, Nagoya University, Nagoya, Japan and UNESCO, p 273
Tu CC, Chen YL, Lin PL, Huang MQ (2022) Analysis and simulations of a heavy rainfall event associated with the passage of a shallow front over Northern Taiwan on 2 June 2017. Mon Wea Rev 150:505–528
Wang B (2006) The Asian Monsoon. Springer-Praxisr, Berlin/Heidelberg, Germany
Wang CC (2015) The more rain, the better the model performs—the dependency of quantitative precipitation forecast skill on rainfall amount for typhoons in Taiwan. Mon Wea Rev 143:1723–1748. https://doi.org/10.1175/MWR-D-14-00137.1
Wang CC, Kuo HC, Yeh TC, Chung CH, Chen YH, Huang SY, Wang YW, Liu CH (2013) High-resolution quantitative precipitation forecasts and simulations by the Cloud-Resolving Storm Simulator (CReSS) for Typhoon Morakot (2009). J Hydrol 506:26–41. https://doi.org/10.1016/j.jhydrol.2013.02.018
Wang CC, Paul S, Chien FC, Lee DI, Chuang PY (2017) An evaluation of WRF rainfall forecasts in Taiwan during three Mei-yu seasons from 2008 to 2010. Wea Forecasting 32:1329–1351
Wang CC, Chang CS, Wang YW, Huang CC, Wang SC, Chen YS, Tsuboki K, Huang SY, Chen SH, Chuang PY, Chiu H (2021b) Evaluating quantitative precipitation forecasts using the 2.5 km CReSS model for typhoons in Taiwan: an update through the 2015 season. Atmosphere 12:1501
Wang CC, Li MS, Chang CS, Chuang PY, Chen SH, Tsuboki K (2021a) Ensemble-based sensitivity analysis and predictability of an extreme rainfall event over Northern Taiwan in the Mei-yu season: the 2 June 2017 case. Atmos Res 259:105684. https://doi.org/10.1016/j.atmosres.2021.105684
Wang AH, Wang CC, Chen GTJ (2021) A study on synoptic conditions leading to the extreme rainfall in Taiwan during 10–12 June 2012. Atmos 12:1255. https://doi.org/10.3390/atmos12101255
Wang CC, Chuang PY, Chang CS, Tsuboki K, Huang SY, Leu G-CGC (2022b) Evaluation of Mei-yu heavy-rainfall quantitative precipitation forecasts in Taiwan by a cloud-resolving model for three seasons of 2012-2014. Nat Hazards Earth Syst Sci 22:23–40. https://doi.org/10.5194/nhess-22-23-2022
Wang CC, Kuo HC, Chen YH, Chen SH, Tsuboki K (2022a) A decade after Typhoon Morakot (2009): what have we learned about its physics and predictability? Wea Forecasting 37:2161–2181. https://doi.org/10.1175/WAF-D-21-0197.1
Wang CC, Chen SH, Chen YH, Kuo HC, Ruppert JH, Tsuboki K (2023c) Cloud-resolving time-lagged rainfall ensemble forecasts for typhoons in Taiwan: examples of Saola (2012), Soulik (2013), and Soudelor (2015). Wea Clim Extremes 40:100555. https://doi.org/10.1016/j.wace.2023.100555
Wang CC, Chen SH, Chuang PY, Chang CS (2023a) Quantitative precipitation forecasts using numerical models: The example of Taiwan. In: Park SK (ed) Numerical Weather Prediction: East Asian Perspectives. Springer. https://doi.org/10.1007/978-3-031-40567-9
Wang CC, Yeh TY, Chang CS, Li MS, Tsuboki K, Liu CH (2023b) A modeling study of an extreme rainfall event along the Northern coast of Taiwan on 2 June 2017. Atmos Chem Phys 23:501–521. https://doi.org/10.5194/acp-23-501-2023
Wang CC, Chien CW, Soong WK, Chen SH (2025a) Evaluation of 8-day typhoon quantitative precipitation forecasts in Taiwan by the 2.5-km CReSS model: overall performance during 2012–16 and impact of domain size. J Hydrometeorol 26:91–110. https://doi.org/10.1175/JHM-D-24-0052.1
Wang CC, Chuang PY, Tsuboki K (2025b) Where and why do Mei-yu season heavy-rainfall quantitative precipitation forecasts in Taiwan improve the most using a higher model resolution? Nat Hazards 121:383–403. https://doi.org/10.1007/s11069-024-06825-5
Wilks DS (2011) Statistical methods in the atmospheric sciences. (3rd ed.) Elsevier, p 467
Wu CC, Kuo YH (1999) Typhoons affecting Taiwan—current understanding and future challenges. Bull Am Meteorol Soc 80:67–80
Yang MJ, Cheng MD, Liou YC, Bell MM, Tsuboki K, Lin PL, Huang CY, Kuo HC, Lin PH, Lee CS, Wang CC, Liu CH, Lu KC, Chang PL, Huang TS, Hou JP, Chung KS, Chang WY, Yang SC, Su SH, Lin PF (2026) Taiwan Area Heavy rain Observation

and Prediction Experiment (TAHOPE): Overview and some scientific results (under review, Terr Atmos Oceanic Sci)
Yeh HC, Chen YL (1998) Characteristics of the rainfall distribution over Taiwan during TAMEX. J Appl Meteorol Clim 37:1457–1469. https://doi.org/10.1175/1520-0450(1998)037%3c1457:CORDOT%3e2.0.CO;2
Yu CK, Cheng LW (2013) Distribution and mechanisms of orographic precipitation associated with Typhoon Morakot (2009). J Atmos Sci 70:2894–2915
Yuan H, McGinley JA, Schultz PJ, Anderson CJ, Lu C (2008) Short-range precipitation forecasts from time-lagged multimodel ensembles during the HMT-West-2006 campaign. J Hydrometeorol 9:477–491. https://doi.org/10.1175/2007JHM879.1
Zhou T, Hsu HH, Matsumoto J (2011) Summer monsoons in East Asia, Indochina and the western North Pacific. In: Chang CP, Ding Y, Lau NC, Johnson RH, Wang B, Yasunari T (eds) The global monsoon system: research and forecast, 2nd ed. World Scientific, Singapore, pp 43–72

Publisher's Note